MULTI-HOP HYBRID FSO/RF COMMUNICATION SYSTEMS

A Thesis

by

Hossein Kazemi

Submitted to the
Graduate School of Sciences and Engineering
In Partial Fulfillment of the Requirements for
the Degree of

Master of Science

in the
Department of Electrical and Electronics Engineering

Özyeğin University
August 2014

MULTI-HOP HYBRID FSO/RF COMMUNICATION SYSTEMS

Approved by:

Professor Murat Uysal, Advisor
Department of Electrical and Electronics Engineering
Özyeğin University

Professor Cenk Demiroğlu
Department of Electrical and Electronics Engineering
Özyeğin University

Dr. Sultan Aldirmaz
Department of Electronics and Communication Engineering
Kocaeli University

Date Approved: 1 August 2014

To my parents ...

ABSTRACT

The reliability of free-space optical (FSO) links is severely restricted by weather-dependent atmospheric phenomena including absorption, scattering and turbulence. An efficient solution is to build hybrid links where a radio frequency (RF) link is incorporated in parallel to the FSO link. With respect to weather conditions, FSO links are mostly degraded by fog and turbulence-induced fading (scintillation) whereas RF links particularly suffer from rain scatter. Therefore, hybrid FSO/RF systems can offer significant enhancements in the system reliability for all weather conditions by means of the complementary nature of the underlying links.

In this thesis, we investigate the outage performance of point-to-point hybrid FSO/RF systems as well as multi-hop hybrid FSO/RF systems with soft-switching. Starting from the point-to-point system, we model the link selection required for soft-switching between the FSO and RF channels in different weather conditions by a finite-state Markov chain (FSMC) process. Then, based on the proposed model, we derive a closed-form outage probability expression in terms of various system and weather-dependent parameters. Thereupon, we extend the scope of our analysis to multi-hop hybrid FSO/RF systems. We present the outage probability and diversity gain analysis for multi-hop hybrid FSO/RF systems. Our results clearly demonstrate the robust performance of the soft-switching hybrid FSO/RF systems deployed either as the point-to-point or multi-hop configuration in dealing with different weather conditions.

ÖZETÇE

Açık uzay optik bağlantılarının (FSO) güvenirliliği absorpsiyon, dağılma ve türbülans gibi atmosferik hava olayları tarafından oldukça kısıtlanmaktadır. Radyo frenkans (RF) bağlantıları ile FSO linklerinin paralel kullanılarak, hibrit bağlantılar inşa edilmesi, bu sorun için verimli bir çözüm olarak ortaya çıkmaktadır. Hava şartları açısından, FSO bağlantıları özellikle sis ve türbülans nedenli zayıflamadan (parıldama) etkilenirken, RF bağlantıları çoğunlukla yağmurdan etkilenir. Bundan dolayı, hibrit FSO/RF sistemleri bütün hava koşullarında oldukça etkin bir gelişim sunar.

Bu tez, noktadan-noktaya hibrit FSO/RF sistemlerinin kesinti performansının yanı sıra, yumuşak anahtarlama ile çoklu atlama hibrit sistemlerinin incelenmesi üzerine yazılmıştır. Noktadan-noktaya sisteminden başlanılarak, sonlu Markov Chain (FSMC) işlemi kullanılmış ve yumuşak anahtarlama için, farklı hava koşulları altında, FSO ve RF kanalları arasında gerekli olan bağlantı seçimleri modellenmiştir. Önerilen modele bağlı kalınarak, çeşitli sistem ve hava koşullarına bağlı parametreler bazında, kapalı-form kesinti olasılık terimi elde edilmiştir. Daha sonra, analizlerin kapsamı çoklu atlama hibrit FSO/RF sistemleri olarak genişletilmiştir. Elde edilen sonuçlar farklı hava şartlarında, yumuşak anahtarlama hibrit FSO/RF sistemlerinin noktadan-noktaya ve çoklu atlama formatlarında etkili bir performans ortaya koyduğunu göstermektedir.

ACKNOWLEDGEMENTS

It is my pleasure to acknowledge all the people who have contributed to this research and my overall experience at OzU.

First and foremost, I would like to take this opportunity to offer my sincere gratitude to my research advisor, Prof. Murat Uysal, for his persistent support, continuous guidance, and invaluable advice during this program. I attribute the level of my Master's degree to his encouragement and effort.

Special thanks go to all my friends especially my lab mates, who provided a perfect environment for my studies and research.

Last but not least, I would like to express my deepest gratitude to my parents. Thanks for their generous and endless love to me. They are always with me whenever I go through tough situations and provide encouragement and support. Without their support, this research work would not happen. My most heartfull appreciation goes to them by dedicating this thesis to them.

Thanks are also due to TUBITAK Research Grant 111E143 for providing financial support during the course of this research.

TABLE OF CONTENTS

LIST OF TABLES

LIST OF FIGURES

CHAPTER I

INTRODUCTION

1.1 Contributions of the Thesis

The main contributions of this thesis can be summarized as follows:

- We analyze the outage probability of a point-to-point hybrid free-space optical/ radio frequency (FSO/RF) system with soft-switching. We first model the link selection required for soft-switching between the FSO and RF channels by a finite-state Markov chain (FSMC) process. Then, based on the proposed model, we derive closed-form outage probability expressions for the hybrid FSO/RF system in terms of various system and weather condition parameters.
- We extend the scope of our analysis to be applied to multi-hop relaying communication systems. For multi-hop hybrid FSO/RF systems, we first investigate the optimum scenario in the sense that the end-to-end outage probability is minimized. Then, based on the outage probability of the optimum scenario, we find the diversity gain of multi-hop hybrid FSO/RF systems through asymptotic analysis.

1.2 Thesis Organization

The remainder of this thesis is organized as follows:

In chapter 2, a detailed description of the point-to-point hybrid FSO/RF system is presented. This includes functional block diagram of the hybrid FSO/RF system, flowchart of the link selection algorithm with hard-switching and soft-switching approaches, signal models for FSO and RF subsystems, path loss and weather-dependent attenuation models, statistical fading distribution models for FSO and RF channels

and statistics of the received SNR for FSO and RF subsystems.

In chapter 3, outage analysis of the point-to-point hybrid FSO/RF communication system is presented. The analysis is based on the proposed FSMC model for soft-switching between the FSO and RF subsystems, which is provided in this chapter. This involves both outage probability and outage capacity results.

In chapter 4, the outage performance of multi-hop hybrid FSO/RF systems is investigated. In this regard, first the detailed analysis for different multi-hop relaying scenarios is presented and the optimum scenario is deduced. Then, diversity gain results for the multi-hop hybrid FSO/RF system through asymptotic analysis is presented.

Finally, the thesis is concluded in chapter 5.

CHAPTER II

THE POINT-TO-POINT HYBRID FSO/RF SYSTEM

In this chapter, a detailed description of the point-to-point hybrid FSO/RF system is presented. In the following sections, first of all, the motivation for how hybrid FSO/RF systems are created, is justified. Then, the functional block diagram of the hybrid FSO/RF system is briefly explained. Subsequently, the flowchart of link selection algorithm with hard-switching and soft-switching approaches is introduced. Thereupon, the signal models for FSO and RF subsystems are individually discussed. Free space path loss and weather-dependent attenuation models as well as statistical fading distribution models for FSO and RF channels are provided. Finally, the statistics of the received SNR for FSO and RF subsystems are derived. This chapter is the basis for the remainder of the thesis since the models presented here are repeatedly used throughout the thesis.

2.1 Background

Free-space optical (FSO) communication technology uses line-of-sight (LOS) propagation of light beams through the atmosphere to realize high-speed optical data communications [1]. The FSO technology combines fiber-bandwidth with the flexibility of wireless [2]. Commercially available FSO systems support data rates of multiple gigabits per second (Gbit/s). Accordingly, it has recently attracted considerable attention as a viable candidate for different applications such as last-mile network access connectivity, fiber optic back-up, cellular backhaul and high speed video transmission, for distances of 4km or less [3].

Despite the major advantages of FSO systems, their reliability is severely restricted by weather-dependent atmospheric phenomena including absorption, scattering and

turbulence. Specifically, the size of fog droplets is typically distributed between 1 to 20 μm, and will effectively scatter all the wavelengths of 0.785, 0.85 and 1.55 μm. In other words, atmospheric attenuations can vary from 0.2 dB/km in exceptionally clear weather to 350 dB/km in very dense fog. This severe attenuation level due to the visibility-limiting weather condition can potentially reduce the up-time or link availability of FSO systems. To meet the five nines carrier-class availability (i.e., 99.999%) requirement, FSO communication range is limited to a very short distance of 140 m in dense fog conditions [4].

To resolve the reliability restriction problem, having a radio-frequency (RF) link and FSO link in tandem works particularly well, since millimeter wave (MMW) transmissions in the RF link are more degraded by rain rather than fog. In fact, rain droplets vary in size from 100 μm to 10 mm, which will effectively scatter MMWs especially those with carrier frequencies of greater than 10 GHz. This gives rise to so-called *hybrid FSO/RF* communication system. The only weather condition that may affect the transmission of a hybrid FSO/RF system is the event when heavy rain and thick fog coincide. However, these two conditions would not occur simultaneously, because as the rain falls, its droplets would absorb the suspended fog water droplets, thus diminishing the fog. Therefore, hybrid FSO/RF systems can offer significant enhancements in the system reliability for all weather conditions by means of the complementary nature of the underlying links.

2.2 System Model

2.2.1 Block Diagram of Hybrid FSO/RF System

The block diagram of the hybrid FSO/RF system is shown in Fig. 1. This system consists of FSO and RF subsystems. Both transmitters are fed from the same information source and they send the data over the channel with their respective rates. In the outage decision block, the SNR levels of FSO and RF links are compared

with their specified values. Then, a system outage is decided in accordance with the comparison result as will be explained in the next chapter.

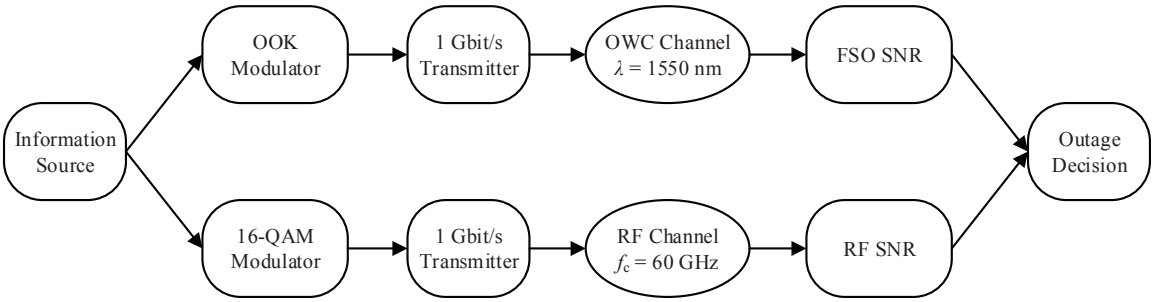

Figure 1: Block diagram of the soft-switching hybrid FSO/RF system.

2.2.2 Link Selection Algorithm

In hybrid FSO/RF systems, there are two principal approaches for channel selection between the FSO and RF links. They are known as hard-switching and soft-switching. Initial works on hybrid FSO/RF links deploy hard-switching approach by which the RF link is used as a fail-over in the case of FSO link failures. A key drawback of this approach is that at a certain time only one link is active providing the data transmission. Once the RF channel is chosen, the capacity of the FSO channel is totally wasted. On the other hand, in soft-switching approach, both links might be active relying on their availabilities whereby data transmission is coordinated through both links [5]. This fully exploits the capacity of both channels and maximizes the average throughput for all weather conditions [6]. The soft-switching hybrid FSO/RF systems can be practically implemented using adaptive modulation and coding [7], as well as channel coding schemes such as convolutional coding [8], low density parity check codes (LDPC) [9], turbo codes [10], hybrid channel codes [11], and Raptor codes [5].

The logical flowchart of link selection algorithm based on soft-switching is illustrated in Fig. 2. This flowchart has been originally proposed in [6] as a bandwidth efficient switch-over algorithm. As observed in Fig. 2, the signal level at the receive

ends should be monitored according to certain thresholds. When the received signal level of the FSO link falls below the threshold, the system performs a switch-over from FSO to RF, similar to the hard-switching method. In this case, the data is sent over the RF link whereas the test data is transmitted through the FSO link. The received signal strength of the FSO link is continuously monitored and compared with the threshold to detect its recovery. If so, the hybrid FSO/RF system will return to its maximum throughput mode by activating both links. The same strategy is applied in case of RF link failure by monitoring the received signal strength of the RF link against the corresponding threshold. When both of the FSO and RF links are down, the system sends test data on both channels in order to detect the recovery for any of links. The switching threshold must be carefully adjusted to ensure that the switching process is initiated and completed before the actual event of FSO or RF link failure [12].

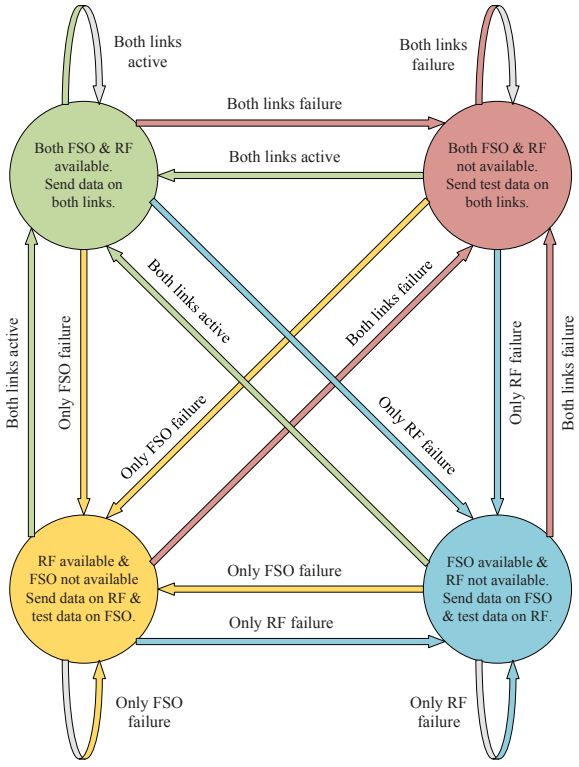

Figure 2: Flowchart of the link selection algorithm based on soft-switching [6].

2.3 Signal and Channel Models

The FSO subsystem uses intensity modulation with direct-detection (IM/DD). The received optical power is detected by a photodiode which produces a photocurrent in proportion to the incident optical power. Afterward, the photocurrent is integrated over one symbol interval and the constant bias by virtue of background radiation is filtered out. We assume operation in high SNR so that the shot noise caused by ambient light is dominant. As a result, Gaussian noise model can be used as a convenient approximation for the Poisson photon counting process.

The received electrical signal is modeled as

$$r_1 = \Re h_1 x_1 + n_1 \tag{1}$$

where $\Re$ is the photodetector responsivity and n_1 is the real-valued zero-mean white Gaussian noise with variance of $\sigma_{n_1}^2 = E[n_1^2]$. In (1), $x_1 \in \{0, 2P_1\}$ is on-off keying (OOK) symbol selected equally likely where P_1 denotes the average transmit optical power (per bit) and h_1 denotes irradiance of the FSO channel which is factored as

$$h_1 = h_{\ell 1} h_{f1} \tag{2}$$

where $h_{\ell 1}$ and h_{f1} are path loss and turbulence-induced fading, respectively.

The path loss factor in (2) aggregates the effect of both geometric loss and atmospheric attenuation. Geometric loss arises due to divergence of the optical beam with respect to the line-of-sight (LOS) and increases with propagation distance. It is a fixed loss for a given FSO link independent of weather conditions. Atmospheric attenuation occurs as a result of scattering and absorption and it is commonly modeled by the exponential Beers-Lambert law. For a point-to-point FSO link, assuming perfect alignment exists between the transmitter and receiver and Gaussian beam profiles, $h_{\ell 1}$ can be approximated as [13]

$$h_{\ell 1} = \left[erf\left(\sqrt{\frac{A_r}{2(\theta L)^2}} \right) \right]^2 e^{-\alpha_1 L} \tag{3}$$

where $erf(.)$ is the error function, $A_r = \pi D^2/4$ is the area of the receive aperture in m^2 with D as the diameter in m, θ is the beam divergence angle in rad, L is the link distance in km, and α_1 is the weather-dependent extinction coefficient in km^{-1}. Alternatively, a more simplified model is available for the path-loss factor as [14]

$$h_{\ell 1} = \frac{A_r}{(\theta L)^2} e^{-\alpha_1 L} \tag{4}$$

For clear or foggy weather, the specific attenuation (i.e., attenuation per unit length) is given by Kim's model as [15, Eq. 10]

$$\alpha_{1,fog} = \frac{3.91}{V} \left(\frac{\lambda_1}{\lambda_0} \right)^{-q} \tag{5}$$

where V is the visibility range in km, λ_1 is the optical wavelength in nm, $\lambda_0 = 550$ nm is the reference wavelength and the parameter q is a piecewise linear function of the visibility range according to

$$q = \begin{cases} 1.6, & 50 < V < \infty \\ 1.3, & 6 < V < 50 \\ 0.16V + 0.34, & 1 < V < 6 \\ V - 0.5, & 0.5 < V < 1 \\ 0, & 0 < V < 0.5 \end{cases} \tag{6}$$

Under rainy weather conditions, the extinction coefficient is given by [16]

$$\alpha_{1,rain} = 1.07 R^{0.67} \qquad \text{in dB/km} \tag{7}$$

with respect to the rainfall rate R in mm/h. Notice that different weather conditions can be classified given the visibility range according to the International Visibility Code weather conditions and precipitation [4]. They are specified in Table 6 of Appendix A. The coefficient h_{f1} in (2) is a random variable identifying the turbulence-induced fading whose models for different turbulence regimes are discussed in the following.

For weak turbulence regime, the fading coefficient has been conventionally modeled by a Log-normal distribution. The probability density function (PDF) of h_{f1} under this model is given by [1]

$$f_{h_{f1}}(h_{f1}) = \frac{1}{2h_{f1}\sqrt{2\pi\sigma_X^2}} \exp\left[-\frac{(\ln h_{f1} - 2\mu_X)^2}{8\sigma_X^2}\right], \quad h_{f1} > 0 \tag{8}$$

where μ_X and σ_X^2 are the mean and the variance of log-amplitude fluctuations, respectively. For weak turbulence, σ_X^2 is related to scintillation index denoted as σ_I^2 through $\sigma_X^2 \approx \sigma_I^2/4$ [1]. To ensure that the fading neither attenuates nor amplifies the average optical power, the fading coefficient is normalized such that $E[h_{f1}] = 1$, implying $\mu_X = -\sigma_X^2$. The scintillation index defined as the normalized variance of irradiance fluctuations at the receive aperture is expressed as [1]

$$\sigma_I^2 = \frac{E[h_{f1}^2] - E^2[h_{f1}]}{E^2[h_{f1}]} \tag{9}$$

where $E(.)$ denotes the expectation operator. For the aperture-averaged spherical wave, the scintillation index is given as [17, Eq. 41]

$$\sigma_I^2 = \exp\left[\frac{0.49\chi^2}{(1 + 0.18d^2 + 0.56\chi^{12/5})^{7/6}} + \frac{0.51\chi^2\big(1 + 0.69\chi^{12/5}\big)^{-5/6}}{1 + 0.90d^2 + 0.62d^2\chi^{12/5}}\right] - 1 \tag{10}$$

where $d = \sqrt{\kappa D^2/(4L)}$ and $\chi^2 = 0.4\sigma_R^2$. Here, $\sigma_R^2 = 1.23\kappa^{7/6}C_n^2L^{11/6}$ stands for the Rytov variance where $\kappa = 2\pi/\lambda_1$ is the wavenumber, λ_1 is the optical wavelength in m, and C_n^2 is the index of refraction structure parameter in $\text{m}^{-2/3}$ and is altitude-dependent. One may characterize the weak and strong turbulence regimes by verifying the conditions $\sigma_R^2 < 1$ and $\sigma_R^2 > 1$, respectively. Several C_n^2 profile models are available in the literature, but the most commonly used is the Hufnagle-Valley model described by [17, Eq. 33]

$$\begin{aligned} C_n^2(h) = {} & 0.00594(v/27)^2\big(10^{-5}h\big)^{10}\exp\left(h/1000\right) \\ & + 2.7\times10^{-6}\exp\left(-h/1500\right) + A\exp\left(-h/100\right) \end{aligned} \tag{11}$$

where h is the altitude in meters, v is the rms wind speed in meters per second (m/sec), and $A = C_n^2(0)$ is the ground level value of C_n^2 in $\text{m}^{-2/3}$. For terrestrial FSO

links of up to few kilometers, C_n^2 turns out to be constant along the propagation path and it is commonly adopted as a measure for the turbulence strength. In general, C_n^2 varies from 10^{-17} m$^{-2/3}$ to for weak turbulence to 10^{-13} m$^{-2/3}$ for strong turbulence with 10^{-15} m$^{-2/3}$ often defined as a typical average value [18]. Notice that C_n^2 is weather-dependent which means that the turbulence strength depends on weather conditions too. The values of C_n^2 for a variety of weather conditions used in this thesis are presented in Table 2.

For strong turbulence regime, the Gamma-Gamma distribution is more successful to fit the experimental data. In fact, the Gamma-Gamma fading model is valid for a wide range of turbulence conditions from weak to strong regimes [19]. Under this model, the PDF of h_{f1} is given by [19]

$$f_{h_{f1}}(h_{f1}) = \frac{2(\alpha\beta)^{(\alpha+\beta)/2}}{\Gamma(\alpha)\Gamma(\beta)} h_{f1}^{(\alpha+\beta)/2-1} K_{\alpha-\beta}\left(2\sqrt{\alpha\beta h_{f1}}\right), \qquad h_{f1} > 0 \tag{12}$$

where $\Gamma(z) = \int_0^\infty e^{-t}t^{z-1}dt$ is the Gamma function, and $K_v(\cdot)$ is the v^{th} order modified Bessel function of the second kind [20, Eq. 8.407-1]. In (12), the positive parameters α and β are linked to the scintillation index in (9) through $\sigma_I^2 = 1/\alpha + 1/\beta + 1/(\alpha\beta)$. Assuming spherical wave propagation, α and β can be directly linked to physical parameters via [17, Eqs. 60, 61]

$$\alpha = \left[\exp\left(\frac{0.49\chi^2}{\left(1 + 0.18d^2 + 0.56\chi^{12/5}\right)^{7/6}}\right) - 1\right]^{-1} \tag{13}$$

$$\beta = \left[\exp\left(\frac{0.51\chi^2\left(1 + 0.69\chi^{12/5}\right)^{-5/6}}{1 + 0.90d^2 + 0.62d^2\chi^{12/5}}\right) - 1\right]^{-1} \tag{14}$$

2.3.1 RF Subsystem

The RF subsystem uses a line-of-sight (LOS) link and operates at the unlicensed MMW band with a carrier frequency of 60 GHz. The choice of the 60 GHz carrier frequency is most suitable to meet the requirement for a powerful RF link with data rates comparable to the FSO counterpart [14]. In addition to the high-data rates

that can be accomplished in this spectrum, energy propagation in the 60 GHz band has unique characteristics that make possible many other benefits such as excellent immunity to interference, high security, and frequency re-use [21]. Besides, the 60 GHz links are carrier-class communication enabled, that is, they can be engineered to deliver five nines of availability if desired [22].

The RF subsystem employs M-ary quadrature amplitude modulation (M-QAM). The constellation size of the QAM modulation is typically chosen as non-binary (i.e., $M > 2$) for bandwidth efficient transmission. The equivalent complex baseband signal at the output of the receiver can be written as

$$r_2 = h_2 x_2 + n_2 \tag{15}$$

where x_2 is the QAM symbol with average power of $E[|x_2|^2] = P_2 \log_2 M$, and n_2 is the noise term assumed to be complex zero-mean white Gaussian with variance of $\sigma_{n_2}^2 = E[|n_2|^2]$. Notice that here P_2 represents the transmit power per bit for the RF subsystem. The RF noise variance is described with [8]

$$\sigma_{n_2}^2 = 10\log_{10}(B) + N_0 + N_F, \quad \text{in dB} \tag{16}$$

where B, N_0 and N_f represent the RF bandwidth in MHz, the noise power spectral density (PSD) in dB/MHz and the receiver noise figure, respectively. In (15), h_2 denotes the RF link channel coefficient which can be factorized as [8]

$$h_2 = \sqrt{h_{\ell 2}} h_{f2} \tag{17}$$

where $h_{\ell 2}$ and h_{f2} denote path loss and fading coefficient, correspondingly. At the 60 GHz frequency, $h_{\ell 2}$ is modeled as [23]

$$h_{\ell 2} = G_t + G_r - 20\log_{10}(4\pi L/\lambda_2) - \alpha_{2,oxy} L - \alpha_{2,rain} L, \quad \text{in dB} \tag{18}$$

in which G_t and G_r stand for the transmit and receive antenna gains, respectively, λ_2 is the RF wavelength and, $\alpha_{2,oxy}$ and $\alpha_{2,rain}$ are the attenuation coefficients due to

oxygen absorption and rain scattering, respectively. For $\alpha_{2,rain}$, a prediction model recommended by ITU-R can be used which is given by [24]

$$\alpha_{2,rain} = aR^b \tag{19}$$

where R is the rainfall rate in mm/h and, the parameters a and b dependent upon the frequency and microstructure of the rain droplets are given by

$$a = \frac{k_H + k_V + (k_H + k_V)\cos^2\varphi\cos 2\tau}{2} \tag{20}$$

$$b = \frac{k_H\alpha_H + k_V\alpha_V + (k_H\alpha_H - k_V\alpha_V)\cos^2\varphi\cos 2\tau}{2a} \tag{21}$$

in which φ is the path elevation angle and τ is the polarization tilt angle relative to the horizontal path. The values of constants k_H, k_V, α_H, α_V up to frequency of 400 GHz are given in ITU-R.

The fading coefficient h_{f2} is modeled by Rician distribution whose PDF is provided by [25, pp. 21]

$$f_{h_{f2}}(h_{f2}) = \frac{2\,(K+1)\,h_{f2}}{\Omega}\exp\left(-(K+1)\frac{h_{f2}^2}{\Omega} - K\right) I_0\left(2\sqrt{K(K+1)\frac{h_{f2}^2}{\Omega}}\right), h_{f2} > 0 \tag{22}$$

where K is the Rician factor, $I_0(.)$ denotes the zeroth order modified Bessel function of the first kind, and Ω is the average fading power. From the energy conservation theorem, it is assumed that $\Omega = E[h_{f2}^2] = 1$. The Rician factor is defined as the ratio between the received power of the line-of-sight (LOS) component to that of the specular (multi-path) components and depends on various link parameters such as link distance or antenna height. We note that as K goes to infinity, the Rician fading coefficient asymptotically approaches unity. Hence, the RF channel will follow a simple additive white Gaussian noise (AWGN) model in this case.

2.3.2 SNR Statistics

Further developments of the analysis in this thesis requires to determine the SNR statistics in terms of the PDF and cumulative distribution function (CDF). Here, the

SNR statistics for both of the FSO and RF subsystems are presented.

Based on (1), the instantaneous electrical SNR of the FSO link is defined as [26]

$$\gamma_1 \triangleq \frac{\left(E\left[\Re h_{\ell 1} h_{f1} x_1 \left| h_{f1} \right.\right]\right)^2}{\sigma_{n1}^2} = \bar{\gamma}_1 h_{f1}^2 \tag{23}$$

where $E[.|.]$ denotes the conditional expectation and $\bar{\gamma}_1$ is the average SNR of the FSO link given by

$$\bar{\gamma}_1 = \frac{\Re^2 h_{\ell 1}^2 P_1^2}{\sigma_{n_1}^2} \tag{24}$$

After a simple transformation of the random variable h_{f1} using (23) in (8), for the case of Log-normal fading, the PDF of γ_1 is derived as

$$f_{\gamma_1}(\gamma_1) = \frac{1}{4\gamma_1 \sqrt{2\pi\sigma_X^2}} \exp\left[-\frac{\left(\ln\left(\gamma_1/\bar{\gamma}_1\right) + 4\sigma_X^2\right)^2}{32\sigma_X^2}\right], \quad \gamma_1 > 0 \tag{25}$$

while its CDF can be expressed as

$$F_{\gamma_1}(\gamma_{th1}) = Q\left(\frac{\ln\sqrt{\bar{\gamma}_1/\gamma_{th1}} - 2\sigma_X^2}{2\sigma_X}\right) \tag{26}$$

where $Q(x) = \left(1/\sqrt{2\pi}\right)\int_x^\infty \mathrm{e}^{-t^2/2} dt$ is the Gaussian Q-function. For the case of Gamma-Gamma fading, similarly, by applying the random variable transformation of (23) in (12), the PDF of can be derived as

$$f_{\gamma_1}(\gamma_1) = \frac{1}{\gamma_1 \Gamma(\alpha)\Gamma(\beta)} \left(\alpha\beta\sqrt{\frac{\gamma_1}{\bar{\gamma}_1}}\right)^{\frac{\alpha+\beta}{2}} K_{\alpha-\beta}\left(2\sqrt{\alpha\beta\sqrt{\frac{\gamma_1}{\bar{\gamma}_1}}}\right), \quad \gamma_1 > 0 \tag{27}$$

and the CDF of γ_1 can be found as

$$F_{\gamma_1}(\gamma_{th1}) = \frac{1}{\Gamma(\alpha)\Gamma(\beta)} G_{1,3}^{2,1}\left[\alpha\beta\sqrt{\frac{\gamma_{th1}}{\bar{\gamma}_1}} \,\middle|\, \begin{matrix} 1 \\ \alpha, \beta, 0 \end{matrix}\right] \tag{28}$$

where $G_{p,q}^{m,n}[\cdot]$ represents the Meijer's G-function as defined in [20, Eq. 9.301]. A proof for the derivation of (28) has been provided in Appendix B.

On the other hand, based on (15), the instantaneous electrical SNR of the RF link is defined as [7]

$$\gamma_2 \triangleq \frac{E\left[\left|\sqrt{h_{\ell 2}} h_{f2} x_2\right|^2 \left| h_{f2} \right.\right]}{\sigma_{n_2}^2} = \bar{\gamma}_2 h_{f2}^2 \tag{29}$$

where $\bar{\gamma}_2$ represents the average SNR of the RF link which is obtained as

$$\bar{\gamma}_2 = \frac{h_{\ell 2} P_2 \log_2 M}{\sigma_{n_2}^2} \tag{30}$$

Notice that $\bar{\gamma}_2$ is the average SNR per QAM symbol. Instead, should we need the average SNR per bit for the RF link, it is equal to $\bar{\gamma}_2/\log_2 M$. Performing the random variable transformation of (29) on (15), the PDF of γ_2 can be derived as [25, pp. 420]

$$f_{\gamma_2}(\gamma_2) = \frac{K+1}{\bar{\gamma}_2} \exp\left(-(K+1)\frac{\gamma_2}{\bar{\gamma}_2} - K\right) I_0\left(2\sqrt{K(K+1)\frac{\gamma_2}{\bar{\gamma}_2}}\right), \quad \gamma_2 > 0 \tag{31}$$

Moreover, the CDF of γ_2 can be written in the form

$$F_{\gamma_2}(\gamma_{th2}) = 1 - Q_1\left(\sqrt{2K}, \sqrt{2(K+1)\frac{\gamma_{th2}}{\bar{\gamma}_2}}\right) \tag{32}$$

in which $Q_1(x,y) = \int_y^\infty t \exp[-(t^2+x^2)/2] I_0(xt) dt$ is the first-order Marcum Q-function.

2.4 Numerical Results

2.4.1 Numerical Assumptions

The numerical assumptions presented here are globally adopted throughout the thesis except otherwise declared. We assume the deployment of OOK and rectangular 16-QAM modulation schemes for the FSO and RF subsystems, correspondingly. The FSO transmitter operates at 1 Gbit/s while the RF one operates at 250 Msym/s implying an effective data rate of 1 Gbit/s as can be seen in Fig.1. A target BER of $BER_T = 10^{-9}$ is considered for the system reliability, which implies an equivalent threshold SNR of about 16 dB for both the FSO and RF subsystems.

The values of relevant system parameters and the weather-dependent variables for the FSO and RF subsystems are extracted from [4], [8], [13], [15], [24] and tabulated in Tables 1 and 2, respectively. From Table 2, it is noteworthy that there is a high degree of inverse correlation between the turbulence strength C_n^2 and attenuation level in the FSO channel. For example, the value of C_n^2 in a clear weather is much higher

comparing to that in adverse weather conditions. Conversely, strong turbulence is highly unlikely to occur during a foggy high-loss event as can be seen in Table 2.

Table 1: Parameters of FSO and RF subsystems [8], [13].

FSO Subsystem		
Parameter	**Symbol**	**Value**
Modulation	–	OOK
Wavelength	λ_1	1550 nm
Responsivity	R	0.5 A/W
Noise variance	σ_{n1}^2	10^{-14} A^2
Beam divergence angle	θ	2 mrad
Receiver aperture diameter	D	20 cm
RF Subsystem		
Modulation	–	16-QAM
Carrier frequency	f_c	60 GHz
Bandwidth	B	250 MHz
Transmitter antenna gain	G_t	44 dBi
Receiver antenna gain	G_r	44 dBi
Oxygen attenuation	$\alpha_{2,\text{oxy}}$	15.1 dB/km
Rician factor	K	6 dB
Noise PSD	N_0	-114 dB/MHz
Receiver noise figure	N_F	5 dB

Table 2: Weather-dependent variables [4], [15], [24].

Weather Condition		Rain Rate	$C_n^2 \times 10^{-14}$ [m$^{-2/3}$]	α_1 [dB/km]	α_2 [dB/km]
1	Clear air	–	5.0	0.43	0
2	Haze	–	1.7	3.34	0
3	Light fog	–	0.3	16.67	0
4	Moderate fog	–	0.2	35.38	0
5	Heavy fog	–	0.1	113.20	0
6	Light rain	2.5 mm/h	0.6	1.98	1.50
7	Moderate rain	12.5 mm/h	0.5	5.84	5.69
8	Heavy rain	25 mm/h	0.4	9.29	10.09

2.4.2 Average SNRs of FSO and RF Subsystems

Here, we present our numerical results for average SNR analysis of the FSO and RF links based on (24) and (30). For a fair comparison, average SNR curves are plotted versus the total transmit power per bit P_t with equal transmit power allocations for the FSO and RF subsystems so that $P_1 = P_2 = P_t/2$. We assume a fixed total transmit power of $P_t = 20$ mW and allow for the link distance to vary. Figs. 3 and 4 demonstrate average SNR/bit of the FSO and RF subsystems as a function of the link distance in different foggy and rainy weather conditions, respectively.

As Fig. 3 represents, average SNR of the FSO link is rapidly dropping as the fog thickness is increased. For moderate and heavy fog conditions, the FSO link distance is limited to very short ranges while the RF link has still a qualified average SNR. More specifically, in heavy fog conditions, the FSO link is not usable since its average SNR is quickly dropped to zero for a link distance of less than 300 m.

On the other hand, as Fig. 4 shows, average SNR of the RF link is more reduced more than that of the FSO link in rainy weather conditions. This is because of the fact that the RF link has higher attenuation levels in rain with respect to the FSO link. However, under heavy rain conditions, the average SNR for both links are almost equal over the shown link range.

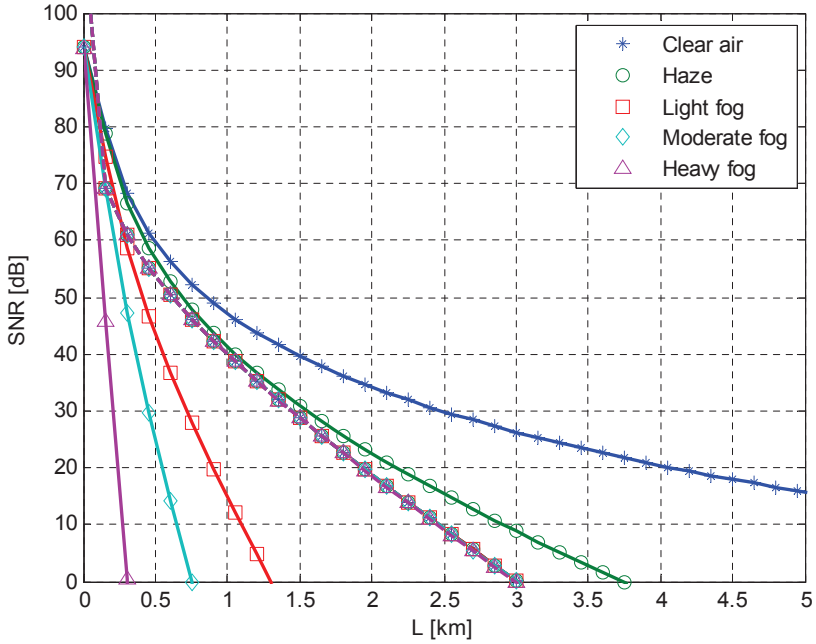

Figure 3: Average SNR/bit of FSO $\bar{\gamma}_1$ (solid lines) and RF $\bar{\gamma}_2/\log_2 M$ (dashed lines) subsystems as a function of link distance L in different foggy weather conditions.

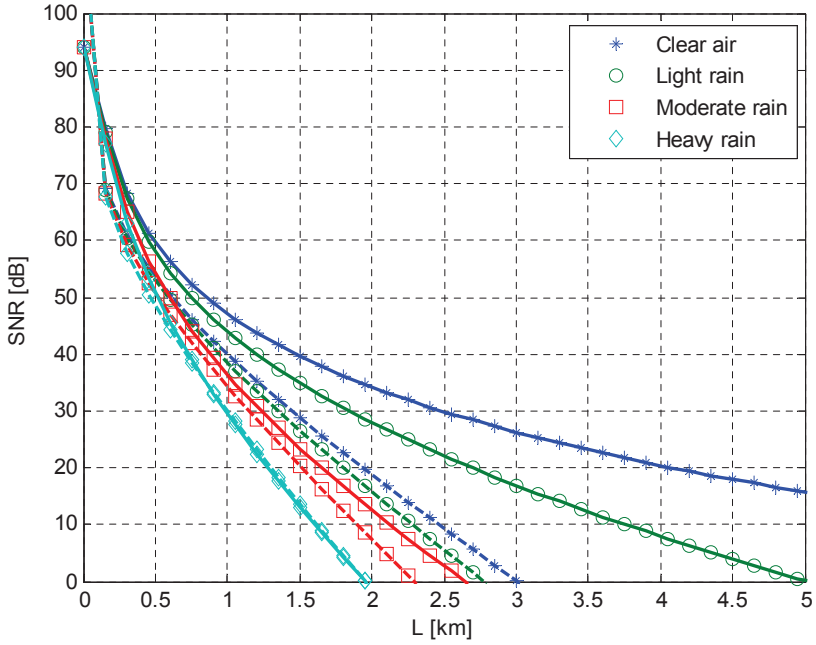

Figure 4: Average SNR/bit of FSO $\bar{\gamma}_1$ (solid lines) and RF $\bar{\gamma}_2/\log_2 M$ (dashed lines) subsystems as a function of link distance L in different rainy weather conditions.

CHAPTER III

OUTAGE ANALYSIS OF HYBRID FSO/RF SYSTEM

In this chapter, the outage probability of the point-to-point hybrid FSO/RF communication system with soft-switching is analyzed. In soft-switching approach, either one of the links or both links can be active based on their availabilities in different weather conditions. First, the link selection required for soft-switching between the FSO and RF channels is modeled by a finite-state Markov chain (FSMC) process. Then, based on the proposed model, closed-form outage probability expressions are derived in terms of various system and weather condition parameters. Furthermore, outage capacity of the hybrid FSO/RF system is analyzed using the FSMC model. Numerical results are provided to present the outage performance under a variety of weather conditions.

3.1 Background

In the current chapter, we present the link selection modeling and outage performance analysis for the point-to-point hybrid FSO/RF system described in chapter 2. First, we establish an important model based on FSMC process which is a foundation for the remainder of this thesis for performance analysis purposes. In this regard, the references [27] and [28] were brought to our attention. In [27], the authors have considered hard-switching instead of soft-switching, and suggested to model the underlying link selection process by an FSMC with three states. However, their primary observation for an always-active RF link cannot be a realistic assumption and hence the presented results are questionable. The authors in [28] have proposed an FSMC model for a hybrid FSO/MMW RF channel from an upper-layer network perspective. More specifically, they have mathematically analyzed the hybrid FSO/RF system as

a queuing system with two inhomogeneous service rates. Though their model is an adequate choice for packet flow analysis in a data communication network, it is not a pertinent model for the physical layer performance evaluation of hybrid FSO/RF systems.

There are some efforts in the literature to study the outage probability of hybrid FSO/RF systems either theoretical [29], [30] or experimental [31]. However, there does not exist any closed-form analytical outage probability expression for hybrid FSO/RF systems in the literature to the best of our knowledge. Therefore, we utilize our FSMC model to derive an outage probability expression for the hybrid FSO/RF system under consideration. Subsequently, we derive the channel capacity with outage (i.e., outage capacity) for the soft-switching hybrid FSO/RF system. Notice that the average capacity results in [32] for hard-switching FSO/RF systems were built on the model presented in [28] and thus they are not reliable.

3.2 Finite-State Markov Chain Modeling

In this section, we model the link selection required for soft-switching between the FSO and RF channels in different weather conditions by an FSMC process. Let us define γ_{th1} and γ_{th2} as the threshold SNRs required to satisfy certain levels of bit error rate (BER) for the FSO and RF links, respectively. These thresholds can be found using the following BER expressions corresponding to the FSO and RF subsystems as [33], [25]

$$P_{e,OOK} = Q\left(\sqrt{\gamma_1}\right) \tag{33}$$

$$P_{e,M-QAM} = 4P_b\left(1 - P_b\right), \quad P_b = \left(1 - \frac{1}{\sqrt{M}}\right) Q\left(\sqrt{\frac{3\gamma_2}{M-1}}\right) \tag{34}$$

Evaluating (33) and (34) for $\gamma_1 = \gamma_{th1}$ and $\gamma_2 = \gamma_{th2}$, then solving them for γ_{th1} and γ_{th2} yields

$$\gamma_{th1} = \left[Q^{-1}\left(BER_T\right)\right]^2 \tag{35}$$

$$\gamma_{th2} = \left(\frac{M-1}{3}\right)\left[Q^{-1}\left(\frac{1-\sqrt{BER_T}}{2\left(1-1/\sqrt{M}\right)}\right)\right]^2 \tag{36}$$

where $Q^{-1}(.)$ is the inverse Q-function and BER_T accounts for the target BER.

In a soft-switching system, either link 1 (FSO) or link 2 (RF) or both links might be active as long as the threshold condition, i.e., $\gamma_i > \gamma_{th\ i}$ for $i = 1, 2$, is fulfilled. These comparisons may divide the first quarter of the $\gamma_1\gamma_2$ plane into four disjoint regions of operation where each of them corresponds to a distinct state for the hybrid FSO/RF system as depicted in Fig. 5. Subsequently, using the state labels as shown in Fig. 5, the state diagram of the link selection algorithm including a four-state Markov chain model is illustrated in Fig. 6.

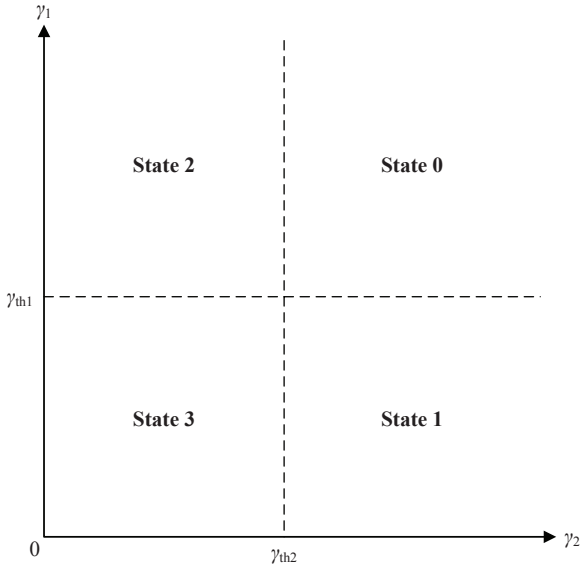

Figure 5: Four disjoint regions in $\gamma_1\gamma_2$ plane based on threshold SNRs.

The status of the switch device at a given time sample n is a discrete random variable denoted by $X_n \in \{0, 1, 2, 3\}$. We assume homogeneous transition probabilities which means that the one-step transition probabilities are fixed and preserved over time. The state transition probabilities are defined as

$$p_{ij} \triangleq \Pr\left\{X_{n+1} = i | X_n = j\right\}, \quad \text{for } i, j \in \{0, 1, 2, 3\} \text{ and for every } n. \tag{37}$$

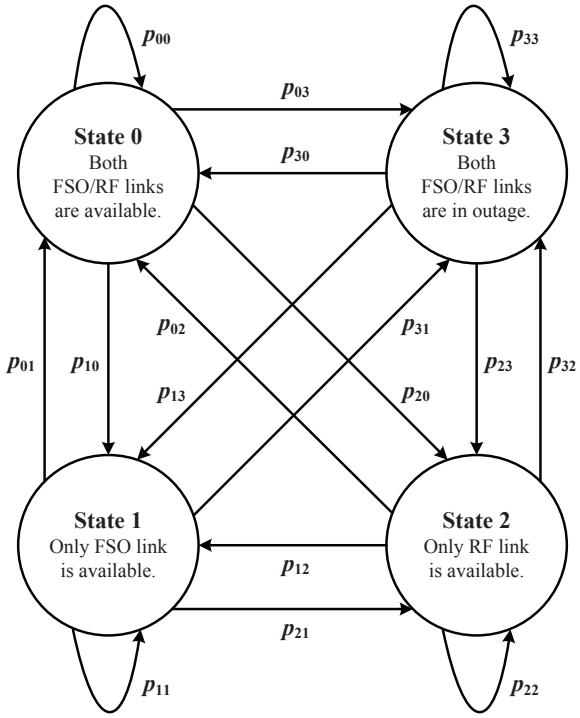

Figure 6: State diagram of the proposed four-state Markov chain model for the soft-switching hybrid FSO/RF system.

Since our model comprises only a single irreducible FSMC as depicted in Fig. 6, there exists a stationary probability mass function (PMF) for it [34]. After the process has been running for a long time (i.e., $n \to \infty$) Markov chain settles into stationary behavior and the n-step transition probability matrix approaches a constant matrix. Therefore, in steady-state the columns of the state transition matrix denoted by $\mathbf{P}$ are all equal to the same PMF. Defining the stationary probability of being at the i^{th} state as π_i, we get

$$p_{i0} = p_{i1} = p_{i2} = p_{i3} = \pi_i, \quad \text{for } i \ = \ 0, 1, 2, 3 \tag{38}$$

where $p_{ij} \triangleq [\mathbf{P}]_{ij}$. Combining (37) with (38), the state transition matrix is simplifie

$$\mathbf{P} = \begin{bmatrix} \pi_0 & \pi_0 & \pi_0 & \pi_0 \\ \pi_1 & \pi_1 & \pi_1 & \pi_1 \\ \pi_2 & \pi_2 & \pi_2 & \pi_2 \\ \pi_3 & \pi_3 & \pi_3 & \pi_3 \end{bmatrix}. \tag{39}$$

Keeping in mind that $\sum_{i=0}^{3} \pi_i = 1$, the matrix given by (39) fulfills fundamental property of a state transition probability matrix, that is, $\sum_{i=0}^{3} p_{ij} = 1$ for $j = 0, 1, 2, 3$. Furthermore, it can be easily verified that $\mathbf{P}\boldsymbol{\pi} = \boldsymbol{\pi}$ where $\boldsymbol{\pi} = [\pi_0 \quad \pi_1 \quad \pi_2 \quad \pi_3 \,]^T$ and $[\cdot]^T$ represents the transpose operation. In other words, the vector $\boldsymbol{\pi}$ is a right eigenvector of $\mathbf{P}$ with a unit eigenvalue. The stationary probabilities can be directly found using their definitions as

$$\pi_0 = \Pr\{\gamma_1 > \gamma_{th1}, \gamma_2 > \gamma_{th2}\} = (1 - F_{\gamma_1}(\gamma_{th1}))(1 - F_{\gamma_2}(\gamma_{th2})) \tag{40}$$

$$\pi_1 = \Pr\{\gamma_1 > \gamma_{th1}, \gamma_2 < \gamma_{th2}\} = (1 - F_{\gamma_1}(\gamma_{th1}))F_{\gamma_2}(\gamma_{th2}) \tag{41}$$

$$\pi_2 = \Pr\{\gamma_1 < \gamma_{th1}, \gamma_2 > \gamma_{th2}\} = F_{\gamma_1}(\gamma_{th1})(1 - F_{\gamma_2}(\gamma_{th2})) \tag{42}$$

$$\pi_3 = \Pr\{\gamma_1 < \gamma_{th1}, \gamma_2 < \gamma_{th2}\} = F_{\gamma_1}(\gamma_{th1})F_{\gamma_2}(\gamma_{th2}) \tag{43}$$

where $F_{\gamma_1}(\cdot)$ and $F_{\gamma_2}(\cdot)$ are given by (26) or (28), and (32) in chapter 2, respectively.

3.3 Outage Probability Analysis

The outage probability is a widely used information-theoretical criterion of wireless systems to assess the performance over quasi-static fading channels [35]. It is defined as the probability that the instantaneous BER exceeds a specified value or equivalently the probability that the output SNR falls below a certain threshold. In this section, we utilize our FSMC model for analyzing the outage probability of the hybrid FSO/RF system.

Let us denote $C(\gamma)$ as the instantaneous channel capacity as a function of the instantaneous electrical SNR γ. The outage probability at a transmission rate of R_0 is defined as [35]

$$P_{out}(\gamma_{th}) \triangleq \Pr\{C(\gamma) < R_0\} = \Pr\{\gamma < \gamma_{th}\} \tag{44}$$

where the second equality comes from the fact that $C(\cdot)$ is monotonically increasing with respect to γ and $\gamma_{th} = C^{-1}(R_0)$ is the threshold SNR. If SNR exceeds γ_{th}, no outage happens and the signal can be decoded with arbitrarily low BER.

We notice that the stationary probabilities given by (40)–(43) imply three different types of outage probability. Let us call π_1 as "RF outage" since it defines the probability that only FSO link is available. Similarly, we call π_2 as "FSO outage" because it returns the probability that only RF link is available. We are particularly interested in π_3 which corresponds to outage probability of the soft-switching hybrid FSO/RF system, abbreviated to "Hybrid outage". The RF outage, FSO outage and Hybrid outage probabilities are denoted by $P_{out,S1}$, $P_{out,S2}$ and $P_{out,Hyb}$, respectively. They can be rewritten as

$$P_{out,S1}(P_1, P_2) = (1 - P_{out,FSO}(P_1))\, P_{out,RF}(P_2), \tag{45}$$

$$P_{out,S2}(P_1, P_2) = P_{out,FSO}(P_1)\,(1 - P_{out,RF}(P_2))\,, \tag{46}$$

$$P_{out,Hyb}(P_1, P_2) = P_{out,FSO}(P_1) P_{out,RF}(P_2) \tag{47}$$

where $P_{out,FSO}(P_1)$ and $P_{out,RF}(P_2)$ are the outage probabilities corresponding to the individual FSO and RF subsystems as the function of their respective transmit powers per bit (i.e., P_1 and P_2). From chapter 2, using (26), (27) and (32) with expanding $\bar{\gamma}_1$ and $\bar{\gamma}_2$ in terms of the transmit powers as defined by (24) and (30), we obtain

$$P_{out,FSO}\,(P_1) = Q\left(\frac{\ln\left(h_{\ell 1} P_1 / P_{th1}\right) - 2\sigma_X^2}{2\sigma_X}\right) \tag{48}$$

for the case of Log-normal fading,

$$P_{out,FSO}\,(P_1) = \frac{1}{\Gamma(\alpha)\Gamma(\beta)} G_{1,3}^{2,1}\left[\frac{\alpha\beta P_{th1}}{h_{\ell 1} P_1}\,\middle|\,\begin{matrix} 1 \\ \\ \alpha, \beta, 0 \end{matrix}\right] \tag{49}$$

for the case of Gamma-Gamma fading, and

$$P_{out,RF}\,(P_2) = 1 - Q_1\left(\sqrt{2K}, \sqrt{2\,(K+1)\,\frac{P_{th2}}{h_{\ell 2} P_2}}\right) \tag{50}$$

In (48)-(50), $P_{th1} \triangleq \sqrt{\gamma_{th1}\sigma_{n1}^2/\Re^2}$ and $P_{th2} \triangleq \gamma_{th2}\sigma_{n2}^2/\log_2 M$ are defined as threshold transmit powers (per bit) required to guarantee the target BERs for the FSO and

RF subsystems, respectively. As a comparative figure of merit (FOM), we consider the critical point at which the outage probability curves of the individual FSO and RF subsystems intersect. The corresponding threshold transmit power is identified by $P_{th,FOM}$ and is equal to solution of the equation $P_{out,FSO}(P_1) = P_{out,RF}(P_2)$ for $P_1 = P_2 = P_{th,FOM}/2$ which can be calculated based on (48) or (49) with (50).

3.4 Outage Capacity Analysis

Channel capacity is the maximum achievable data rate that can be reliably communicated between the transmitter and the receiver [35]. In this section, we apply our FSMC model to derive the outage capacity of the point-to-point hybrid FSO/RF system presented in chapter 2. For quasi-static fading channels considered in this thesis, we assume that the perfect knowledge of the instantaneous fading states (i.e., h_{f1} and h_{f2}) are available at the FSO and RF receivers.

For the FSO subsystem, since we confine our attention to the practical case of equiprobable binary OOK alphabets, capacity refers to the maximum rate using this source distribution. The instantaneous capacity in bits/channel use of the FSO link corresponding to γ_1 is given by [13]

$$C_{FSO}(\gamma_1) = \sum_{x_1} P_X(x_1) \int_{-\infty}^{\infty} f_{r_1|x_1}(r_1|x_1) \log_2 \frac{f_{r_1|x_1}(r_1|x_1)}{f_{r_1}(r_1)} dr_1 \tag{51}$$

where $x_1 \in \{0, 2P_1\}$, $P_X(x_1 = 0) = P_X(x_1 = 2P_1) = 0.5$, $f_{r_1|x_1}(r_1|x_1)$ is a Gaussian probability density function with the mean $\Re h_{\ell 1} h_{f1} x_1$ and the variance $\sigma_{n_1}^2$, and $f_{r_1}(r_1) = \sum_{x_1} P_X(x_1) f_{r_1|x_1}(r_1|x_1)$.

On the other hand, the instantaneous capacity in bits/channel use of the RF link corresponding to γ_2 is given as [9]

$$C_{RF}(\gamma_2) = -\log_2\left(2\pi e \sigma_{n_2}^2\right) - \int_{-\infty}^{\infty} \frac{1}{M} \sum_{x_2} f_{r_2|x_2}(r_2|x_2) \log_2 \left(\frac{1}{M} \sum_{x_2} f_{r_2|x_2}(r_2|x_2) \right) dr_2 \tag{52}$$

where $f_{r_2|x_2}(r_2|x_2) = \left(2\pi\sigma_{n_2}^2\right)^{-1} \exp\left(-\|r_2 - x_2\|^2 / 2\sigma_{n_2}^2\right)$ in which $\|.\|$ is the Euclidean norm and, $x_2 \in S_x$ and S_x is the M-QAM symbol set.

The outage capacity is defined as the average rate of correctly received data over many transmission bursts [35]. It can be expressed as $C_{out} = (1 - P_{out}(\gamma_{th}))\, C(\gamma_{th})$ since data is correctly received only on $1 - P_{out}(\gamma_{th})$ portion of transmissions [35]. Here, $P_{out}(\gamma_{th})$ is defined in (44). Therefore, denoting the i^{th} state of the FSMC model in Fig. 6 by S_i for $i = 0, 1, 2, 3$, the outage capacity of the soft-switching hybrid FSO/RF system represented by $C_{out,Hyb}$ can be expressed as

$$C_{out,Hyb} = \sum_{i=0}^{3} \pi_i C_{Hyb|S_i} \tag{53}$$

where π_i, for $i = 0, 1, 2, 3$, are given by (40)-(43), and $C_{Hyb|S_i}$ is the capacity of the soft-switching hybrid FSO/RF system operating at the state. By inspection of the state-diagram in Fig. 4, it can be observed that

$$C_{Hyb|S_0} = C_{FSO}(\gamma_{th1}) + C_{RF}(\gamma_{th2}) \tag{54}$$

$$C_{Hyb|S_1} = C_{FSO}(\gamma_{th1}) \tag{55}$$

$$C_{Hyb|S_2} = C_{RF}(\gamma_{th2}) \tag{56}$$

$$C_{Hyb|S_3} = 0 \tag{57}$$

Substituting (54)-(57) into (53), the outage capacity of the soft-switching hybrid FSO/RF system is found as

$$C_{out,Hyb}(\gamma_{th1}, \gamma_{th2}) = (\pi_0 + \pi_1)\, C_{FSO}(\gamma_{th1}) + (\pi_0 + \pi_2)\, C_{RF}(\gamma_{th2}) \tag{58}$$

Replacing (40)-(42) in (58), the outage capacity can be further simplified a

$$\begin{aligned} C_{out,Hyb}(\gamma_{th1}, \gamma_{th2}) &= (1 - P_{out,FSO}(\gamma_{th1}))\, C_{FSO}(\gamma_{th1}) + (1 - P_{out,RF}(\gamma_{th2}))\, C_{RF}(\gamma_{th2}) \\ &= C_{out,FSO}(\gamma_{th1}) + C_{out,RF}(\gamma_{th2}) \quad \text{in bits/channel use} \end{aligned} \tag{59}$$

where $C_{out,FSO}(\gamma_{th1}) \triangleq (1 - P_{out,FSO}(\gamma_{th1}))\, C_{FSO}(\gamma_{th1})$ and $C_{out,RF}(\gamma_{th2}) \triangleq C_{RF}(\gamma_{th2})$ $\times (1 - P_{out,RF}(\gamma_{th2}))$ are defined as the outage capacities of the FSO and RF subsystems, correspondingly. The last result in (59) reveals that the outage capacity of the soft-switching hybrid FSO/RF system is equal to the summation of the outage capacities of the individual FSO and RF channels. This shows that the soft-switching hybrid FSO/RF system can optimally achieve the capacity of the combined FSO and RF channels in addition to providing the carrier grade reliability. The fact that has already been conjectured in [36] but not been proved.

3.5 Performance Results and Discussions

In this section, we present our numerical results for outage analysis of the soft-switching hybrid FSO/RF system based on (45)-(47). We consider an end-to-end link distance of $L = 1$ km and allow the transmit power to vary. We assume Log-normal fading for the FSO channel. We use the numerical assumptions for all other parameters and weather-dependent variables as given by Tables 1 and 2 in chapter 2. To make a fair comparison, outage performance curves are plotted versus the total transmit power per bit P_t with equal power allocations for the FSO and RF subsystems so that $P_1 = P_2 = P_t/2$.

The RF outage (i.e., only FSO link is available, $P_{out,S1}$), FSO outage (i.e., only RF link is available, $P_{out,S2}$) and Hybrid outage ($P_{out,Hyb}$) probabilities for clear weather condition are plotted in Fig. 7. It is observed that $P_{out,S1}$ increases with increase in P_t and makes a peak at $P_t = -4.2$ dBm, then starts decreasing. Similarly, $P_{out,S2}$ makes a peak at $P_t = -2.2$ dBm. Note that $P_{out,S1}$ and $P_{out,S2}$ belong to State 1 and State 2 probabilities based on (45) and (46) and are different from the stand-alone (individual) outage probabilities of FSO and RF links (i.e., $P_{out,FSO}$ and $P_{out,RF}$) which are further included for comparison purposes. The distinguishing threshold corresponds to the point of intersection between the RF outage and Hybrid outage

curves with a threshold transmit power of $P_{th0} = -2.7$ dBm. In $P_t < P_{th0}$ region, we observe the probability that the only FSO link is available (RF outage) is lowest. In comparison, the probability that the only RF link is available (FSO outage) stands higher and, with probability very close to one, the RF link is available for $P_t \approx P_{th0}$ as can be verified from Fig. 7. For $P_t > P_{th0}$ region, the best performance is attained by the hybrid system. This, in turn, indicates that for low values of P_t the hybrid FSO/RF system can still rely on the RF link to achieve the "five nines" carrier-class availability (99.999%) [4], which requires an outage probability of at least 10^{-6} [31]. The corresponding transmit power threshold denoted by $P_{th,5N}$ for the RF outage (i.e., only FSO link is available) and Hybrid outage probabilities are found as $P_{th,5N} = -5.4$ and $P_{th,5N} = -0.3$ dBm, respectively.

In the following, we focus only on the outage probability of the soft-switching hybrid FSO/RF system (i.e., Hybrid outage). Fig. 8 exhibits the outage probability in clear weather condition. In this figure, we verify our analytical result in (47) by computer simulation of (43). It can be observed from Fig. 8 that the analytical result perfectly matches with the simulation result.

Outage performance for different foggy weather conditions is demonstrated in Fig. 9. The outage performance in the clear weather is also included as a benchmark. Fig. 9 clearly demonstrates that the hybrid FSO/RF system performs better than the individual FSO and RF links for all fog levels. Also, the more the fog thickness is, the larger the FOM threshold becomes. For the case of light fog, interestingly, the FOM threshold and the point where the desired outage probability level of 10^{-6} occurs for the hybrid FSO/RF system, coincide. The corresponding transmit power threshold is obtained as $P_{th,FOM} = P_{th,5N} = 14.0$ dBm. It is also observed that under heavy fog the FOM threshold is substantially higher than its preceding cases. In this case, $P_{th,FOM} > 100$ dBm, which means that the FSO link is out of service. In such a situation, the RF transmitter must have a transmit power of at least $P_t = 39.6$ dBm

to provide the five nines link availability.

Fig. 10 demonstrates the outage probability of the soft-switching hybrid FSO/RF system for rainy weather conditions. Similar to Fig. 9, the hybrid FSO/RF system has a better outage performance with respect to stand-alone FSO and RF links for all rain levels. In contrast to foggy weather, the FOM threshold values are remarkably smaller for extreme weather conditions specifically for heavy rain rather than heavy fog. Even in the case of heavy rain, as can be observed from Fig. 10, the FOM threshold is as small as $P_{th,FOM} = 6.4$ dBm and with only a small transmit power of $P_t = 6.9$ dBm the link reliability requirement of $P_{out} = 10^{-6}$ is fully satisfied.

Our observations from these results are summarized in Table 3. In this table, the FOM threshold values for the hybrid FSO/RF system in different weather conditions are listed. Notice that the hybrid FSO/RF system can take the advantage of soft-switching for maximizing the effective throughput if both the FSO and RF subsystems are concurrently active. This happens when P_t is set sufficiently greater than $P_{th,FOM}$. Therefore, the difference between $P_{th,FOM}$ and $P_{th,5N}$ (in dB) is an important factor to evaluate the system reliability. By looking at the values listed in Table 3, we realize that these two thresholds are approximately equal except for the case of heavy fog conditions where the imbalance between is about 71.1 dB as the worst case.

Table 3: The values of $P_{th,5N}$ and $P_{th,FOM}$ for the hybrid FSO/RF system in different weather conditions.

	Clear weather	Haze	Light fog	Moderate fog	Heavy fog	Light rain	Moderate rain	Heavy rain
$P_{th,5N}$ [dBm]	-0.3	1.6	14.0	32.3	39.6	-0.3	3.5	6.9
$P_{th,FOM}$ [dBm]	-1.5	1.0	14.0	32.8	110.7	-0.8	3.0	6.4
P_{out} for $P_{th,FOM}$	6.8×10^{-4}	1.5×10^{-4}	2.7×10^{-7}	9.0×10^{-12}	1.0×10^{-26}	1.5×10^{-3}	2.0×10^{-3}	3.8×10^{-3}

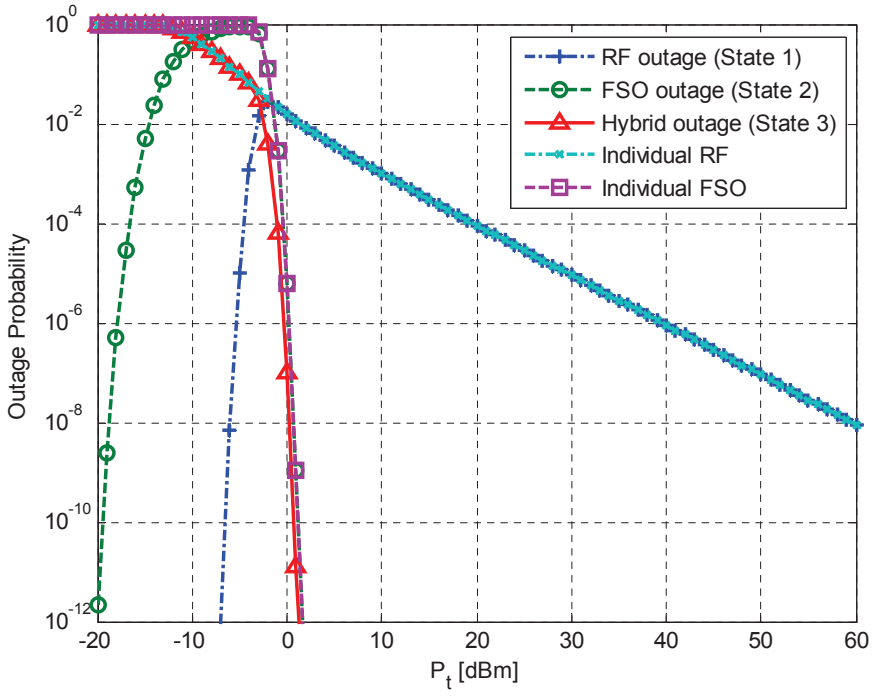

Figure 7: RF outage (i.e., $P_{out,S1}$), FSO outage (i.e., $P_{out,S2}$) and Hybrid outage (i.e., $P_{out,Hyb}$) probabilities under clear weather conditions.

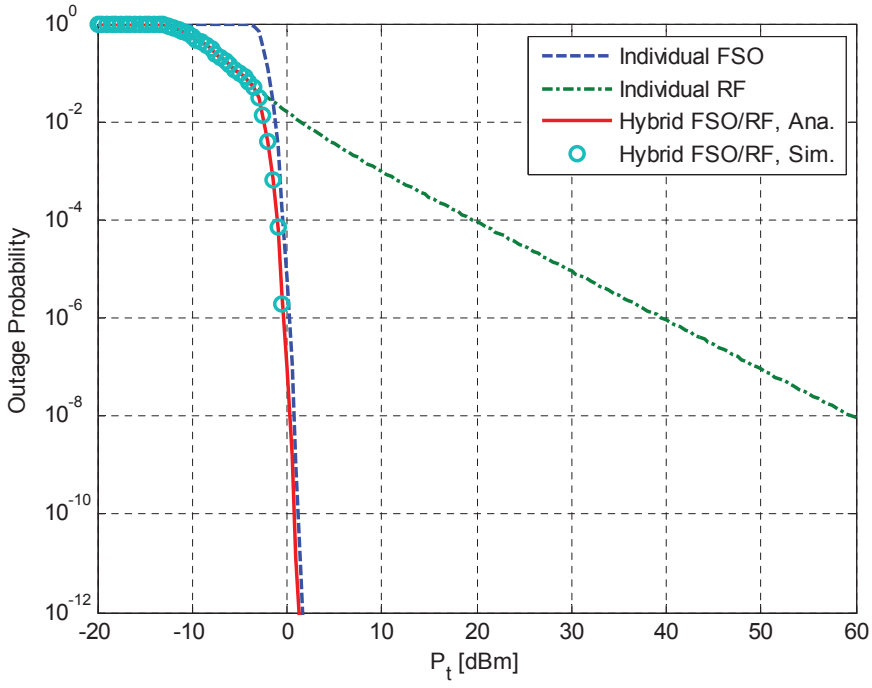

Figure 8: RF outage (i.e., $P_{out,S1}$), FSO outage (i.e., $P_{out,S2}$) and Hybrid outage (i.e., $P_{out,Hyb}$) probabilities under clear weather conditions.

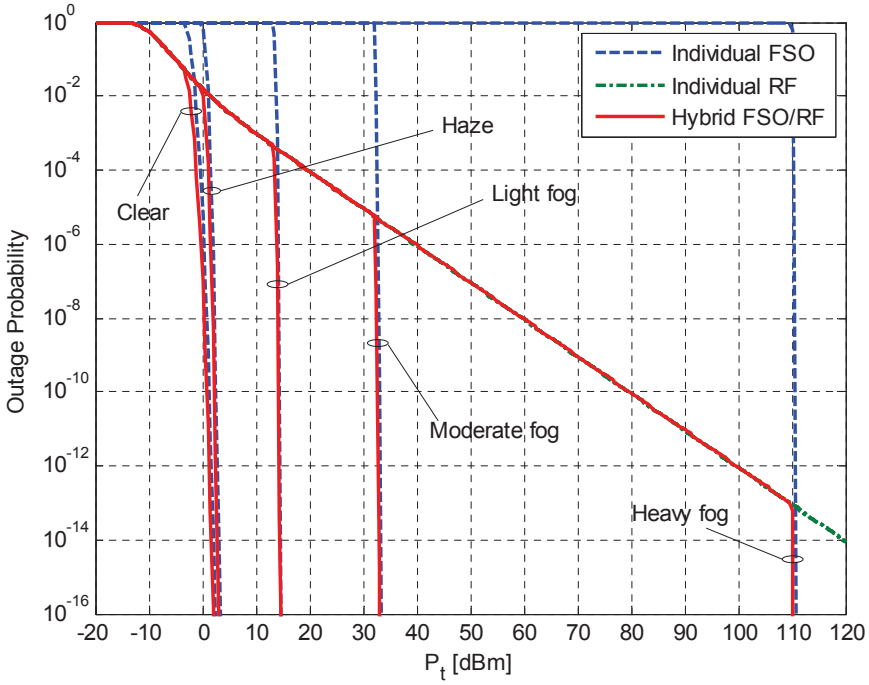

Figure 9: Outage probability of the soft-switching hybrid FSO/RF system under foggy weather conditions.

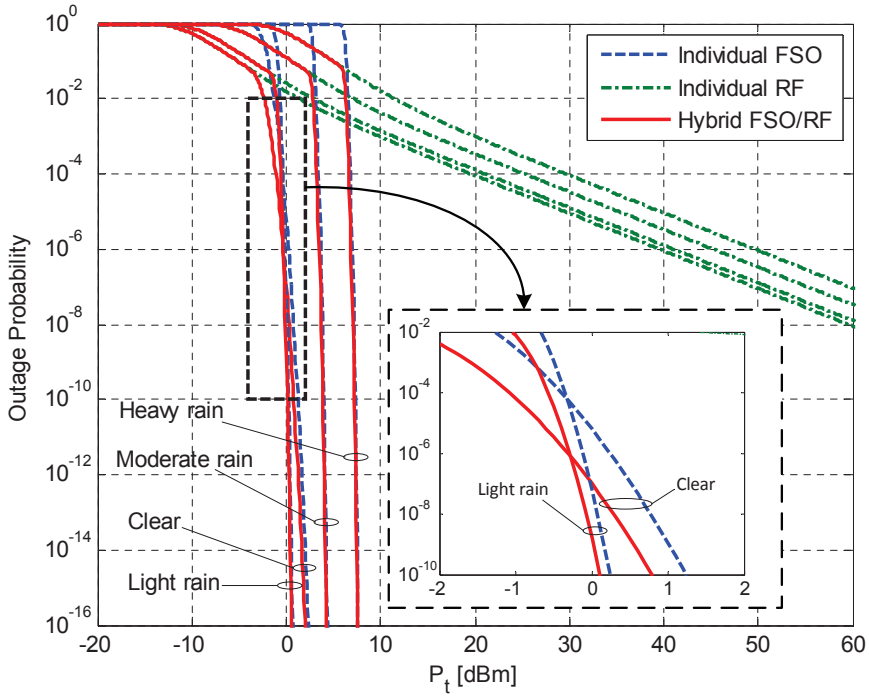

Figure 10: Outage probability of the soft-switching hybrid FSO/RF system under rainy weather conditions.

CHAPTER IV

MULTI-HOP HYBRID FSO/RF SYSTEMS

In this chapter, we intend to extend the scope of our analysis to be applied for multi-hop communications under the assumption of decode-and-forward (DF) relaying protocol. First, several multi-hop hybrid FSO/RF relying scenarios are examined to investigate the optimum multi-hop communication scenario for different weather conditions in the sense of end-to-end outage performance. Thereafter, using the optimum scheme which uses N intermediate hybrid FSO/RF links, we derive the diversity gain of multi-hop hybrid FSO/RF communication system under consideration. For this purpose, we make use of the generalized power series expansion for the outage probability expression and extract the transmit power exponent with asymptotic analysis. As special cases, we further evaluate the derived diversity gain when $D/L \to 0$ in the FSO subsystem (i.e., FSO point receiver) or $N \to \infty$ (i.e., the number of hops is very large). Numerical results are provided to study the outage probability and diversity gain of multi-hop hybrid FSO/RF systems.

4.1 Background

It has been found that multi-hop relaying transmission can bring performance improvements against the degrading effects of fading in FSO communication systems [37]. This is achieved as a result of the ability of relay-assisted transmission with shorter hops to exploit the distance-dependency of FSO fading parameters, cf. (10), (13), (14) in chapter 2.

Multi-hop FSO systems has been extensively studied in the literature (e.g., see [37] and references therein). In [38], multi-hop DF relaying over the atmospheric

poison channel was investigated in terms of the outage probability. In [39], multi-hop FSO communication systems with DF or amplify-and-forward (AF) relaying in strong turbulence channels was analyzed for the end-to-end outage and average bit error probability. In [40], various transmission protocols for relay selection in a dual-hop parallel relaying FSO system with DF relays were studied.

On the other hand, the most severe atmospheric turbulence occurs during only a clear weather condition and, in contrast, the turbulence strength is substantially decreased in a foggy or rainy weather condition. This means that even multi-hop transmission would not be able to improve the reliability of FSO systems especially in foggy weather conditions where the extent of atmospheric attenuation is very high. To overcome this restriction, hybrid FSO/RF links can be incorporated for intermediate hops to enhance the end-to-end reliability of multi-hop communication systems.

The applicability of hybrid FSO/RF links for reliable multi-hop routing in heterogeneous wireless networks has been addressed in [41]. In [42], the per-node throughput capacity of hybrid FSO/RF multi-hop networks has been studied. In [43], the per-node throughput and end-to-end delay of ad-hoc hybrid FSO/RF multi-hop networks have been investigated. Network aspects of hybrid FSO/RF systems have been further studied in the literature in the context of wireless mesh networks (WMNs), e.g. [44–48]. To the best of our knowledge, there is no report in the literature regarding the physical-layer study for end-to-end performance of multi-hop hybrid FSO/RF communication systems. Here, we derive the outage probability and diversity gain expressions and investigate the performance of multi-hop hybrid FSO/RF systems through numerical demonstrations.

4.2 Optimum Multi-Hop Relaying Scenario with Hybrid FSO/RF Links

4.2.1 Considered Scenarios

An outstanding feature of FSO systems is that the fading parameters are distance-dependent, cf. (10), (13), (14) in chapter 2. This allows multi-hop FSO transmission benefit from performance improvements against the degrading effects of turbulence-induced fading, which is a major difference comparing to wireless RF systems [37]. In contrast, RF systems are significantly more stable over adverse weather conditions especially in dense fog. Therefore, we can deploy multi-hop relaying FSO systems to combat the fading effects, while improving the end-to-end link reliability by means of more reliable RF links. A question then arises; what is the optimal multi-hop relying scenario in terms of the number of FSO and RF hops with a fixed service length, in the sense that the outage probability is minimized.

To investigate the aforementioned question, with no loss of generality, we consider a multi-hop transmission scheme comprising three relays in total which can provide at most four hops for each FSO or RF subsystem. Fig. 11 depicts five multi-hop relaying scenarios involving different combinations of FSO and RF links to be analyzed. As a benchmark, the direct transmission from the source to the destination is included as scenario 0 (i.e., reference scenario). We assume the decode-and-forward (DF) relaying protocol for intermediate terminals to forward the signal from the source to the destination over orthogonal time slots [49]. The signal received from the immediate preceding terminal in the current time slot is just decoded and forwarded to the following terminal in the next time slot [50]. Only adjacent terminals can communication with each other while nonadjacent ones are not able to receive the signal from each other. As a result, no multi-hop diversity combining scheme is required at either the intermediate relays or the destination terminal. We further assume the consecutive terminals are placed equidistant along the path from the

source to the destination. For a fair comparison, we always fix the total transmit power (per bit) of the multi-hop hybrid FSO/RF system at P_t and allocate it equally first for intermediate hops and then for FSO and RF subsystems. At the next step, we will present the analytical derivation of the outage probability expressions for these scenarios.

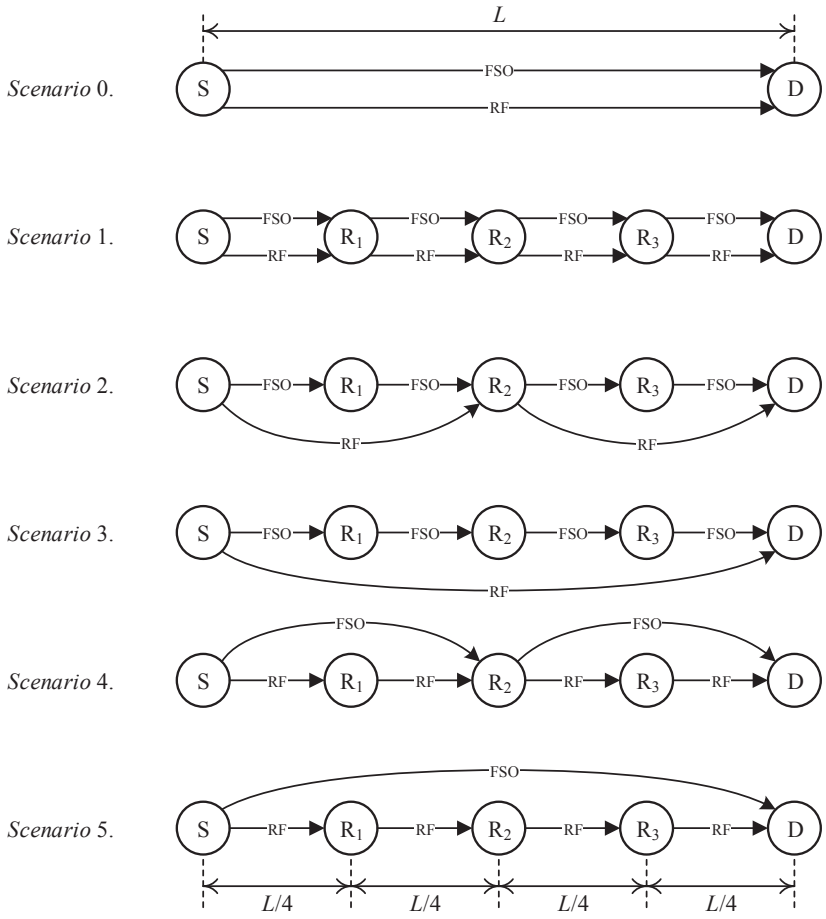

Figure 11: Five scenarios considered for the multi-hop hybrid FSO/RF system.

4.2.2 Outage Probability Analysis

In Fig. 11, scenario 0 represents a single-hop hybrid FSO/RF system lying on the whole end-to-end distance from the source to the destination. For this reference scenario we may recall the outage probability expression earlier found in (47) in

chapter 3 as

$$P_{out} = P_{out,FSO}(L) P_{out,RF}(L) \tag{60}$$

where $P_{out,FSO}(L)$ and $P_{out,RF}(L)$ are outage probabilities of the individual FSO and RF links as a function of the end-to-end link distance. From (48)-(50) in chapter 3, we have

$$P_{out,FSO}(L) = Q\left(\frac{\ln\left(h_{\ell 1}(L) P_1 / P_{th1}\right) - 2\sigma_X^2(L)}{2\sigma_X(L)}\right) \tag{61}$$

for Log-normal fading channel,

$$P_{out,FSO}(L) = \frac{1}{\Gamma(\alpha(L))\Gamma(\beta(L))} G_{1,3}^{2,1}\left[\frac{\alpha(L)\beta(L) P_{th1}}{h_{\ell 1}(L) P_1}\middle| \begin{matrix} 1 \\ \\ \alpha(L), \beta(L), 0 \end{matrix}\right] \tag{62}$$

for Gamma-Gamma fading channel, and

$$P_{out,RF}(L) = 1 - Q_1\left(\sqrt{2K}, \sqrt{2\left(K+1\right)\frac{P_{th2}}{h_{\ell 2}(L) P_2}}\right) \tag{63}$$

In (62) and (63), to emphasize those parameters depending on the link distance we represent them as $h_{\ell 1}(L)$, $\sigma_X^2(L)$, $\alpha(L)$, $\beta(L)$, and $h_{\ell 2}(L)$. Notice that for FSO channel both of the path loss and fading are distance-dependent while for RF channel only the path loss varies with distance as can be observed from (63).

In scenario 1, there is a hybrid FSO/RF link in between every two successive nodes as can be seen from Fig. 11. In this scenario, an outage happens for the end-to-end multi-hop system if any of the intermediate hybrid links is in outage. Hence, the outage probability of scenario 1 can be obtained as

$$P_{out} = \Pr\left\{\bigcup_{i=1}^{4}\left\{i^{th} \text{ hybrid link is in outage}\right\}\right\} \tag{64}$$

The outage probability of scenario 1 in (64) can be rewritten as

$$P_{out} = 1 - \Pr\left\{\bigcap_{i=1}^{4}\left\{i^{th} \text{ hybrid link is available}\right\}\right\} = 1 - \prod_{i=1}^{4}\left(1 - P_{out,Hyb,i}\right) \tag{65}$$

where $P_{out,Hyb,i}$ is the outage probability of the i^{th} hybrid link given by

$$P_{out,Hyb,i} = P_{out,FSO}\left(L/4\right) P_{out,RF}\left(L/4\right) \quad \text{for} \quad i = 1, 2, 3, 4 \tag{66}$$

and $P_{out,Hyb}(\cdot)$ is the outage probability for single-hop hybrid FSO/RF transmission as a function of the link distance.

In scenario 2, FSO links take place in every hop while RF links are located in every other FSO hop. This scenario can be treated as two hops of a single hybrid FSO/RF link where each one consists of two FSO links and one RF link. There exist two of such hybrid links including the one between the nodes S and R_2, and the other one from R_2 to D as shown in Fig. 11. Consequently, for the end-to-end multi-hop system an outage occurs when any of these halfway hybrid links fail. Therefore, the outage probability for scenario 2 can be expressed as

$$P_{out} = \Pr\left\{\bigcup_{i=1}^{2}\left\{i^{th} \text{ hybrid link is in outage}\right\}\right\} \tag{67}$$

The outage probability of scenario 2 in (67) can be simplified as

$$P_{out} = 1 - \Pr\left\{\bigcap_{i=1}^{2}\left\{i^{th} \text{ hybrid link is available}\right\}\right\} = 1 - \prod_{i=1}^{2}\left(1 - P_{out,Hyb,i}\right) \tag{68}$$

where $P_{out,Hyb,i}$ is the outage probability of the i^{th} hybrid link, which can be found as

$$P_{out,Hyb,i} = \left[1 - \left(1 - P_{out,FSO}\left(L/4\right)\right)^2\right] P_{out,RF}\left(L/2\right) \quad \text{for} \;\; i = 1, 2 \tag{69}$$

Scenario 3 can be viewed as a single hybrid link in which the FSO subsystem is composed of four hops and the RF subsystem is arranged as a single communication link connecting the source to the destination. As a result, the outage probability expression of the end-to-end system for scenario 3 is derived as

$$P_{out} = \left[1 - \left(1 - P_{out,FSO}\left(L/4\right)\right)^4\right] P_{out,RF}\left(L\right) \tag{70}$$

We note that the scenarios 4 and 5 resemble the scenarios 2 and 3, respectively. As Fig. 11 clearly illustrates, in these two groups, one scenario may result the other one only by interchanging the roles of FSO and RF subsystems. Therefore, the outage probability expressions for scenarios 4 and 5 are obtained through an exchange of $P_{out,FSO}$ by $P_{out,rF}$ in (68) and (70), respectively. To summarize the outage probability

analysis presented here, the final derived expressions for all of the considered scenarios are listed in Table 4. The required transmit power allocations for hybrid FSO/RF terminals are also included in this table.

Table 4: The outage probability expressions of the considered scenarios along with transmit power allocations for hybrid FSO/RF terminals.

Scenario	Outage Probability Expression	Transmit Power Allocations
0	$P_{out} = P_{out,FSO}(L)P_{out,RF}(L)$	$P_1 = P_2 = P_t/2$
1	$P_{out} = 1-\left[1-P_{out,FSO}\left(L/4\right)P_{out,RF}\left(L/4\right)\right]^4$	$P_1 = P_2 = P_t/8$
2	$P_{out} = 1-\left[\left(1-\left(1-P_{out,FSO}\left(L/4\right)\right)^2\right)P_{out,RF}\left(L/2\right)\right]^2$	$P_1 = P_t/8,\ P_2 = P_t/4$
3	$P_{out} = \left[1-\left(1-P_{out,FSO}\left(L/4\right)\right)^4\right]P_{out,RF}(L)$	$P_1 = P_t/8,\ P_2 = P_t/2$
4	$P_{out} = 1-\left[\left(1-\left(1-P_{out,RF}\left(L/4\right)\right)^2\right)P_{out,FSO}\left(L/2\right)\right]^2$	$P_1 = P_t/4,\ P_2 = P_t/8$
5	$P_{out} = \left[1-\left(1-P_{out,RF}\left(L/4\right)\right)^4\right]P_{out,FSO}(L)$	$P_1 = P_t/2,\ P_2 = P_t/8$

4.2.3 Performance Results

Here, we present our numerical results for outage analysis of different multi-hop hybrid FSO/RF scenarios represented in Fig. 11 based on the derived expressions as given in Table 4. We consider an end-to-end link distance of $L = 2$ km, which yields a length of 500 m for the shortest hop based on the considered scenarios as shown in Fig. 11. For the FSO channel, we assume Log-normal fading. We use the numerical assumptions for all other parameters and weather-dependent variables as given by Table 1 and 2. Outage performance curves are plotted versus to the transmit power per bit P_t with uniform power allocations for intermediate FSO and RF terminals as declared by Table 4. With regard to transmit power allocations reported in Table 4, note that the weighted summation of P_1 and P_2 by the corresponding number of FSO and RF terminals, is equal to P_t for every scenario. Figs. 12-19 demonstrate

the outage probability of multi-hop hybrid FSO/RF scenarios under different weather conditions. For every figure, the outage performance of scenario 0 is included as a benchmark. We observe that the outage performance of the end-to-end system is significantly improved in light of the multi-hop transmission with respect to the reference scenario as shown by Figs. 12-19. In the following, we discuss the performance results separately for different weather conditions.

Fig. 12 illustrates the outage probability of multi-hop hybrid FSO/RF scenarios under clear weather condition. We see that all the outage probability plots have a water-fall curvature. It is observed from Fig. 12 that the overall performance of the end-to-end system is improved for all of the considered multi-hop scenarios with respect to the reference scenario (i.e., scenario 0). However, the extent of the improvement is not identical for different scenarios. In this regard, we may divide up different scenarios into two main categories based on the "breaking point" of their water-fall curves. The breaking point is the point where the water-falling outage curve starts to sharply drop as clearly demonstrated by Fig. 12. Accordingly, the discriminating threshold is set on a transmit power of $P_t = 0$ dBm. The scenarios 1, 2 and 3 have almost the same breaking point in their water-fall curves which is located in the region $P_t < 0$ dBm. The corresponding transmit power is $P_t = -3.1$ dBm. The outage performances of these three scenarios are very close to each other for $P_t > -3.1$ dBm, while they hold different levels for $P_t < -3.1$ dBm. Notice that all of these three scenarios contain four FSO hops, with different numbers of RF hops. For $P_t < -3.1$ dBm, from the highest to the lowest outage probability level, they can be ranked as scenario 3, scenario 2 and scenario 1, respectively. Hence, the more the number of RF hops is, the better the outage performance gets. On the other hand, the breaking points of the scenarios 4 and 5 is occurred for $P_t > 0$ dBm region. While the outage performances of these two scenarios fit together for $P_t < 0$ dBm, they reveal different results for $P_t > 0$ dBm as can be seen from Fig. 12. We note

that both of the scenarios 4 and 5 deploy a constant number of RF hops (i.e., four RF hops), whereas they differ in the number of FSO hops. The outage performance of the scenario 4 with dual-hop FSO transmission is better than the scenario 5 with a single-hop FSO transmission. With reference to the five nines availability [4], [31] (i.e., $P_{out} = 10^{-6}$) target, the scenarios 4 and 5 bring 8.27 dB and 2.31 dB improvement, respectively, in the required transmit power with respect to scenario 0. As a result, the scenario 4 saves about 5.96 dB of transmit power comparing to scenario 5. Meanwhile, the best performance is globally attained by scenario 1 among all of the considered scenarios as can be verified from Fig. 12.

Figs. 13-16 present the outage performance results of multi-hop hybrid FSO/RF scenarios under foggy weather conditions ranging from haze to heavy fog. Let us investigate the carrier class availability (i.e., the five nines availability, 0.99999%) for which an outage probability of $P_{out} = 10^{-6}$ is required. Under light fog conditions, as can be observed from Fig. 14, the scenarios 1, 2 and 3 provide on average 31.85 dB improvement in terms of P_t with respect to scenario 0. The corresponding values for the scenarios 4 and 5 are obtained as 20.40 dB and 1.24 dB. In other words, the scenarios 4 and 5 require 11.85 dB and 30.61 dB more transmit power than the scenarios 1 to 3 to reach at $P_{out} = 10^{-6}$. In heavy fog conditions, as clearly demonstrated by Fig. 16, the scenarios 1, 4 and 5 overlap each other and for the target performance of $P_{out} = 10^{-6}$ they give rise to an improvement of 22.81 dB in the required transmit power with respect to scenario 0. In contrast, using the scenarios 2 and 3 the corresponding improvements are obtained as 15.20 dB and 7.39 dB, respectively. Therefore, the scenarios 2 and 3 need about 7.61 dB and 15.42 dB extra transmit power, correspondingly, to achieve the target outage performance.

Figs. 17-19 present the outage performance results of multi-hop hybrid FSO/RF scenarios under rainy weather conditions ranging from light to heavy rain. Similar

to the case of clear weather condition, the performance results for rainy weather conditions can be studied within two distinct groups, namely, the scenarios 1, 2 and 3 as the first group and, the scenarios 4 and 5 as the second one. Again the target performance of $P_{out} = 10^{-6}$ is considered for comparison purposes. For light rain conditions, the first group provides an average performance improvement of 11.39 dB in terms of the required transmit power with respect to the reference scenario. In comparison, under the same weather conditions, the scenarios 4 and 5 imply 7.01 dB and 0.96 dB improvements, respectively, for the required transmit power with reference to scenario 0. This means, the scenarios 1 to 3 economize on the transmit power by 4.38 dB and 10.43 dB over that required for the scenarios 5 and 6, correspondingly. For moderate and heavy rain conditions, the first group can enhance the end-to-end performance of the system concerning the required transmit power by 17.98 dB and 21.92 dB, respectively, when compared to the reference scenario. With the scenarios 4 and 5, the corresponding values are obtained as 10.72 dB and 1.09 dB for moderate rain and, 14.00 dB and 1.15 dB for heavy rain conditions.

Table 5 summarizes our numerical results for outage analysis of multi-hop hybrid FSO/RF systems deployed with the considered scenarios in different weather conditions. In this table, the values of the required transmit power to guarantee the target outage performance of $P_{out} = 10^{-6}$, are tabulated. Table 5 reveals the superiority of the scenario 1 in comparison with all other scenarios under different weather conditions. Therefore, in conclusion, the scenario 1 is the optimum scenario for the deployment of multi-hop hybrid FSO/RF systems in the sense that the end-to-end system reliability can be effectively improved. However, this favorable result is achieved at the cost of using maximum number of FSO and RF terminals over the link distance from the source to the destination as seen from Fig. 11.

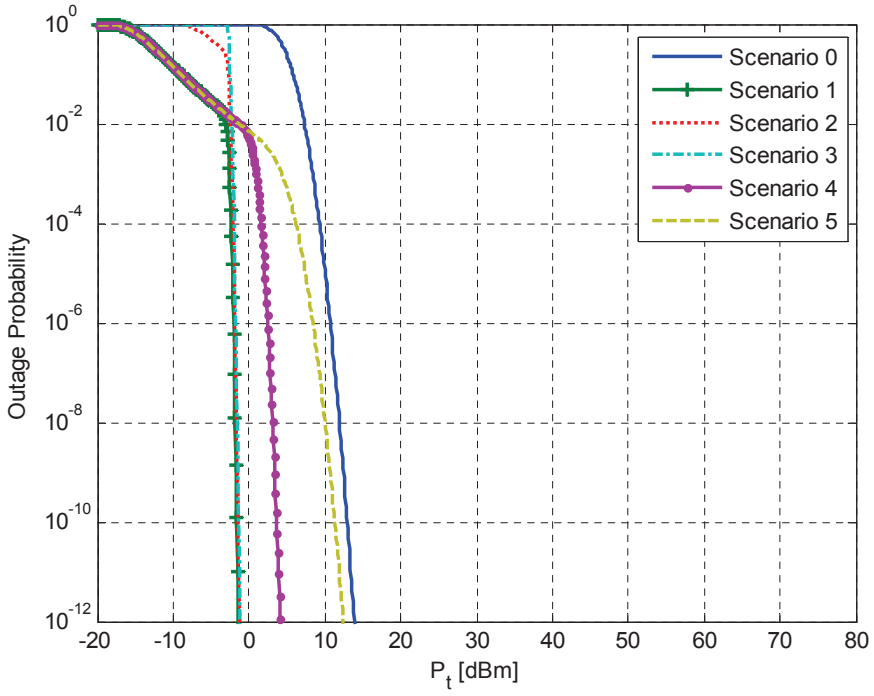

Figure 12: Outage probability of the multi-hop hybrid FSO/RF system with five scenarios under clear weather condition.

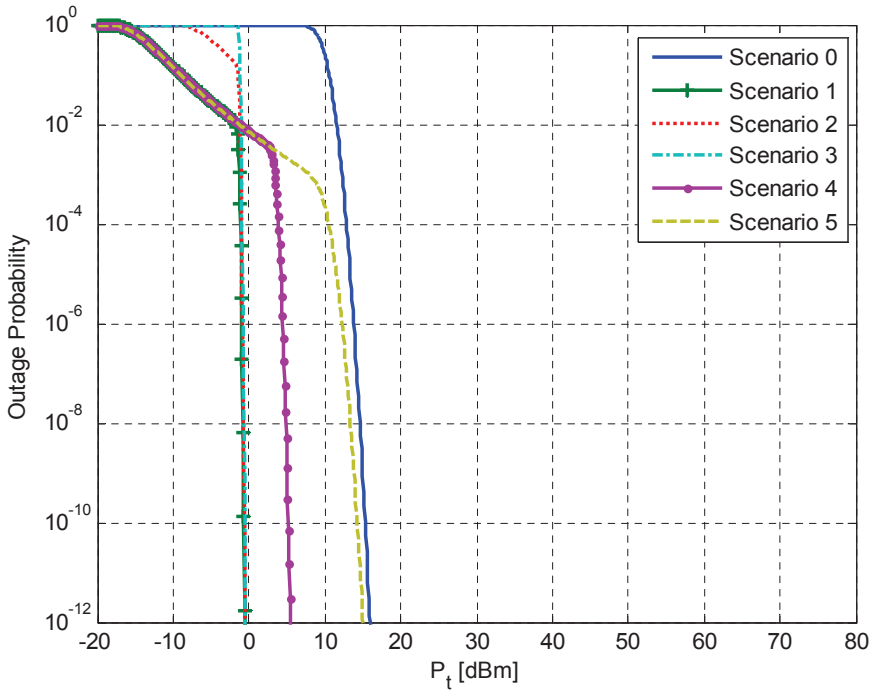

Figure 13: Outage probability of the multi-hop hybrid FSO/RF system with five scenarios under haze conditions.

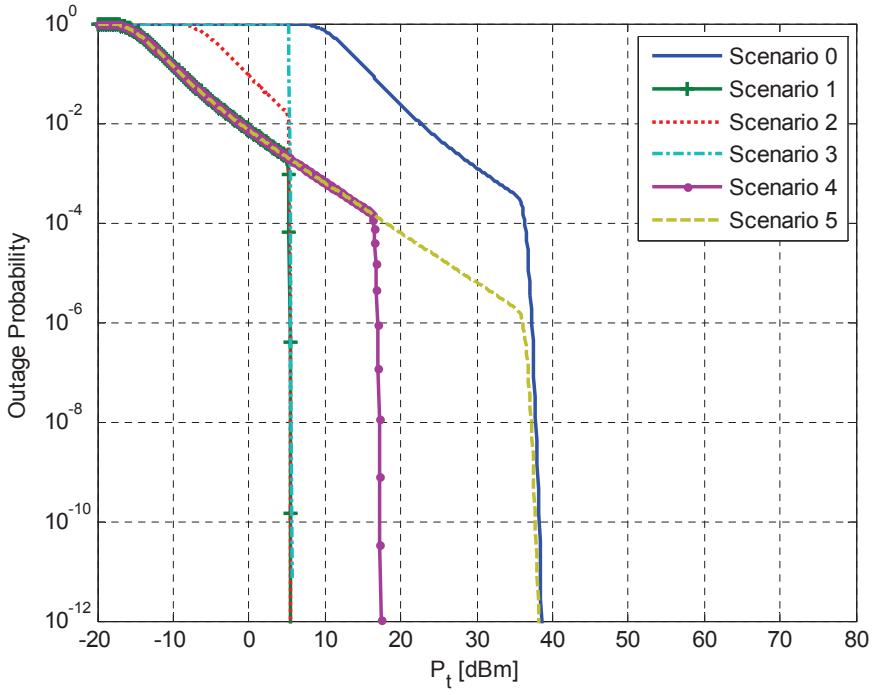

Figure 14: Outage probability of the multi-hop hybrid FSO/RF system with five scenarios under light fog conditions.

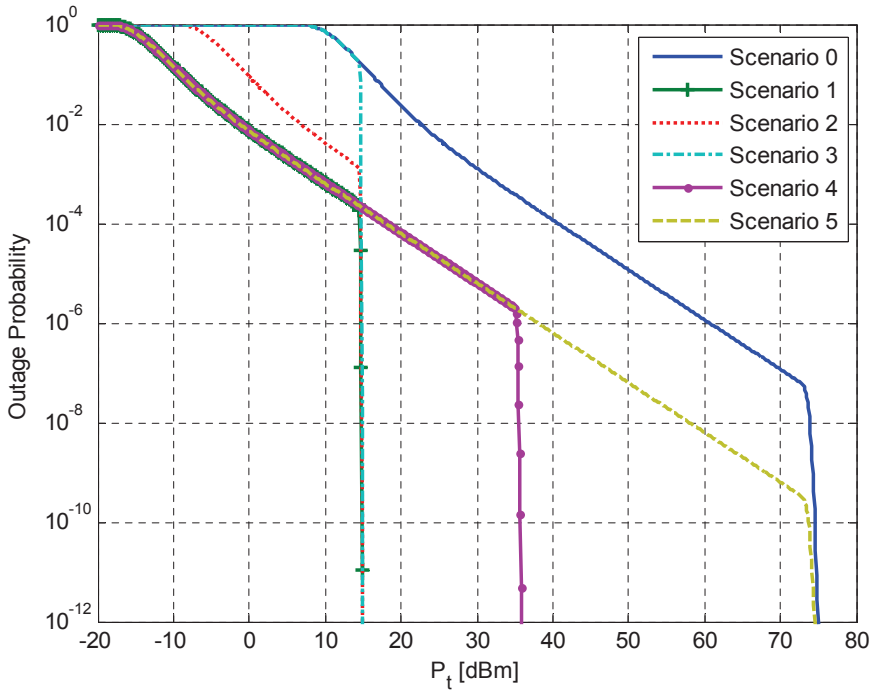

Figure 15: Outage probability of the multi-hop hybrid FSO/RF system with five scenarios under moderate fog conditions.

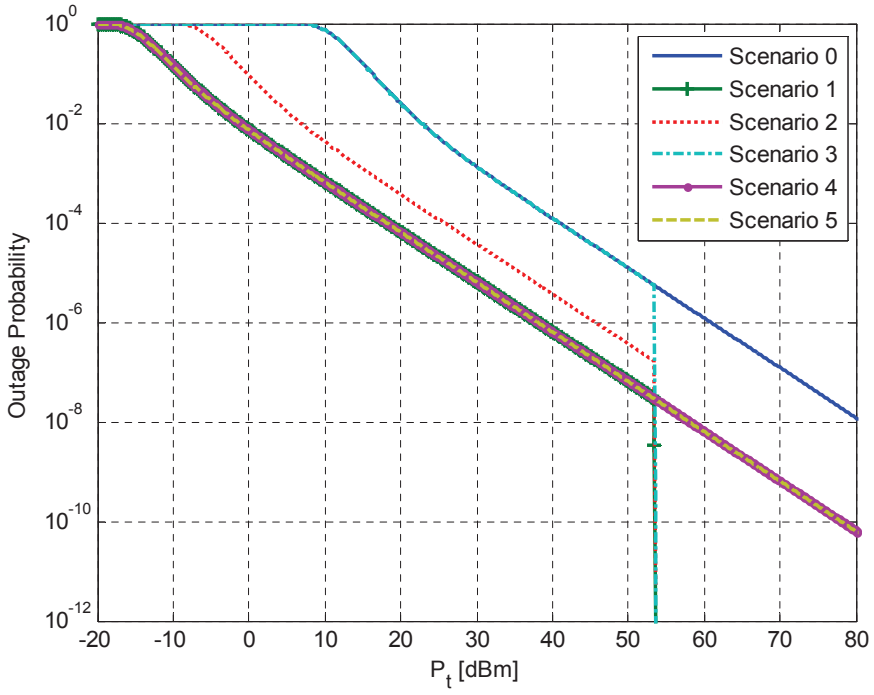

Figure 16: Outage probability of the multi-hop hybrid FSO/RF system with five scenarios under heavy fog conditions.

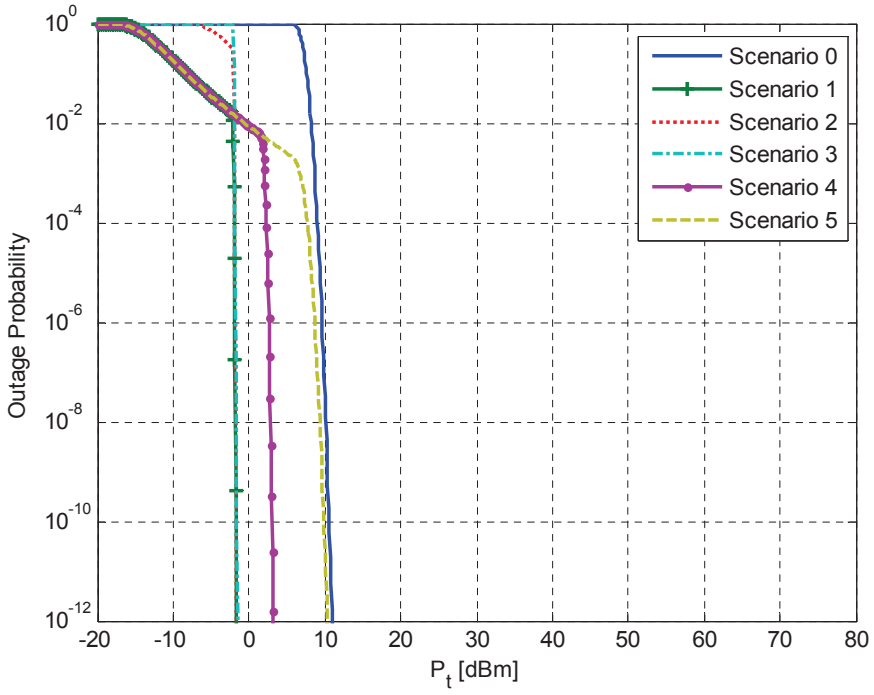

Figure 17: Outage probability of the multi-hop hybrid FSO/RF system with five scenarios under light rain conditions.

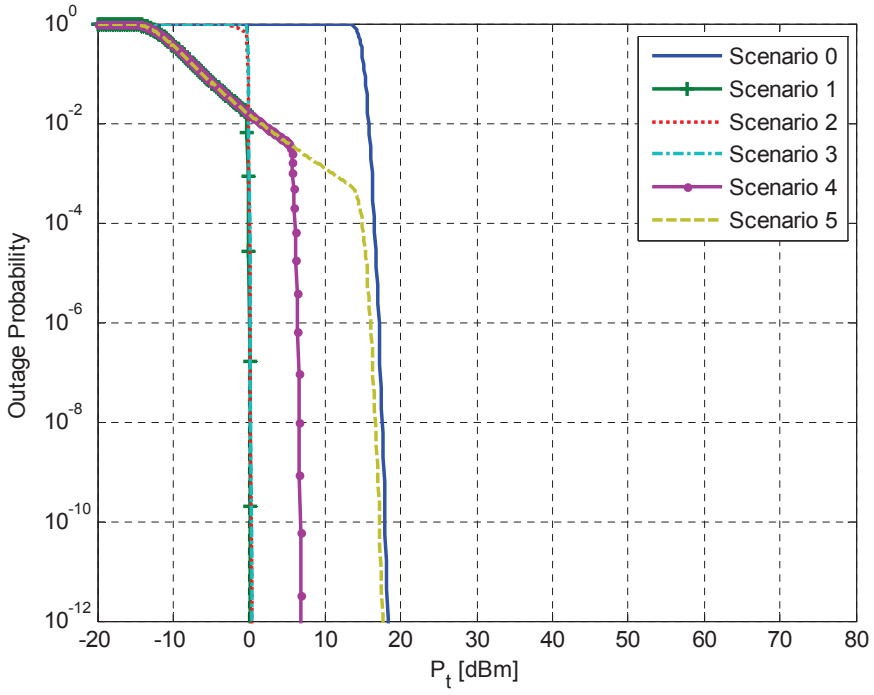

Figure 18: Outage probability of the multi-hop hybrid FSO/RF system with five scenarios under moderate rain conditions.

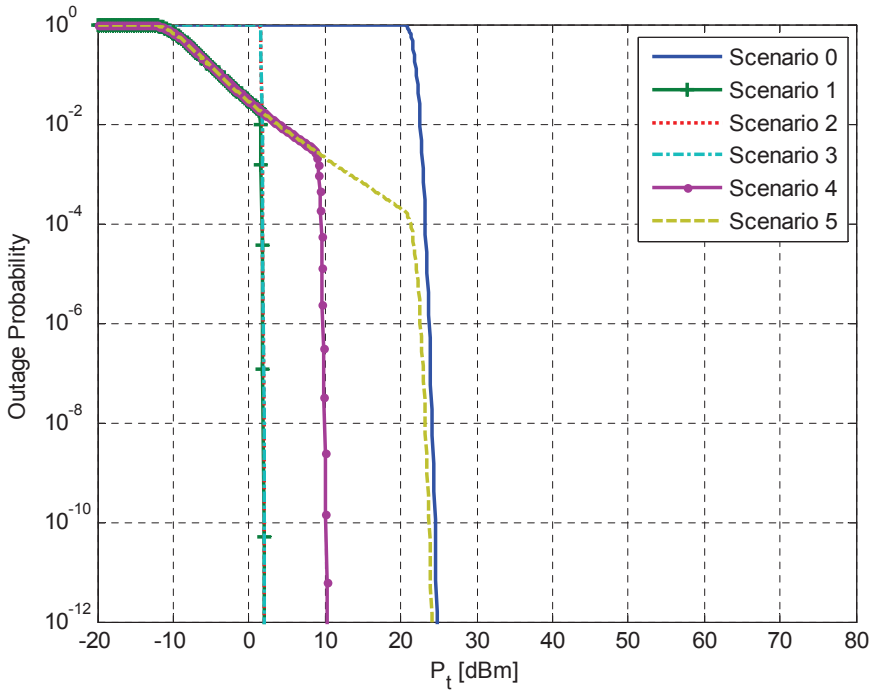

Figure 19: Outage probability of the multi-hop hybrid FSO/RF system with five scenarios under heavy rain conditions.

Table 5: The required P_t [dBm] to achieve the target outage performance of $P_{out} = 10^{-6}$ for multi-hop hybrid FSO/RF scenarios under different weather conditions.

	Clear	**Haze**	**Light fog**	**Moderate fog**	**Heavy fog**	**Light rain**	**Moderate rain**	**Heavy rain**
***Scenario* 0**	10.72	13.80	37.29	60.74	60.91	9.62	17.10	23.74
***Scenario* 1**	-2.03	-0.96	5.39	14.67	38.10	-1.83	0.07	1.77
***Scenario* 2**	-1.85	-0.85	5.43	14.71	45.71	-1.76	0.14	1.84
***Scenario* 3**	-1.73	-0.77	5.49	14.77	53.52	-1.73	0.16	1.85
***Scenario* 4**	2.45	4.44	16.89	35.20	38.10	2.61	6.38	9.74
***Scenario* 5**	8.41	12.25	36.05	38.06	38.10	8.66	16.01	22.59

4.2.4 Outage Probability of the Optimum Scenario

In the previous subsection, we discussed different scenarios for the deployment of multi-hop hybrid FSO/RF systems. At the end, we concluded that the optimum scenario is the one which deploys a hybrid FSO/RF link for every intermediate hop (i.e., scenario 1) to maximize the end-to-end reliability of the system. Hereinafter, we focus only on the optimum scenario in order to further develop the diversity gain analysis for multi-hop hybrid FSO/RF systems that will be presented in section 4.4. To this end, first we need to bring the outage probability expressions and appropriate approximations for it. These are presented in the current subsection and the next section.

In general, we consider the deployment of N relays for multi-hop transmission over the end-to-end link distance of L. The outage probability of the multi-hop hybrid FSO/RF system can be written using (65) as

$$P_{out} = 1 - \prod_{i=1}^{N+1} (1 - P_{out,Hyb,i}) \tag{71}$$

where $P_{out,Hyb,i}$ represents the outage probability of the i^{th} single-hop hybrid FSO/RF link for $i = 1, 2, \ldots, N+1$. Using (60), $P_{out,Hyb,i}$ can be given as

$$P_{out,Hyb,i} = P_{out,FSO}(\ell_i) P_{out,RF}(\ell_i) \tag{72}$$

where ℓ_i is the distance of the i^{th} hybrid link and we have $\sum_{i=1}^{N+1} \ell_i = L$. To make a fair comparison with the direct transmission scheme, we allocate the total available transmit power P_t uniformly among $N+1$ hybrid FSO/RF terminals so that $P_1 = P_2 = P_t \,/\, 2(N+1)$. Here, the division by a factor of 2 arises from equal power allocations for FSO and RF subsystems in every hybrid FSO/RF terminal. In (72), $P_{out,FSO}(\ell_i)$ is given by (61) for Log-normal fading or (62) for Gamma-Gamma fading and, $P_{out,RF}(\ell_i)$ is given by (63).

An upper bound for the outage probability of the multi-hop FSO/RF system is found by expanding the product in (71) and neglecting the higher order terms as

$$P_{out} \leq \sum_{i=1}^{N+1} P_{out,Hyb,i} \tag{73}$$

The upper bound in (73) works very well for a wide range of the total transmit power and gets asymptotically tighter for higher values of P_t. This upper bound will be used subsequently in section 4.4 to do the diversity gain analysis.

4.3 Generalized Power Series Approximations

In this section, we introduce the generalized power series representations for outage probability expressions which is most suitable to derive the diversity gain of the multi-hop hybrid FSO/RF system. In this section, we first work on the point-to-point system whose outage probability is provided by (60). The extension of this analysis to the case of multi-hop systems is presented in the subsequent section. The expression in (60) includes outage probabilities of the FSO and RF subsystems, which are discussed separately in the following.

4.3.1 Outage Probability of FSO Subsystem

For the FSO subsystem, assuming Gamma-Gamma fading channel the corresponding outage probability is given by (62) which involves the evaluation of the Meijer's G-function. Here, we derive a power series expansion for the expression in (62).

Recall from (27) in chapter 2 that the PDF of the instantaneous SNR for the FSO link γ_1 is expressed in terms of the modified Bessel function of the second kind $K_v(\cdot)$. We base our analysis on the generalized power series representation of the modified Bessel function [20, Eqs. 8.445, 8.485], [51, Eq. 6]

$$K_v(x) = \frac{\pi}{2\sin(\pi v)} \left(\sum_{j=0}^{\infty} \frac{1}{\Gamma(j-v+1)j!} \left(\frac{x}{2}\right)^{2j-v} - \sum_{j=0}^{\infty} \frac{1}{\Gamma(j+v+1)j!} \left(\frac{x}{2}\right)^{2j+v} \right) \tag{74}$$

which is valid for $v \notin \mathbb{Z}$ and $|x| < \infty$. Replacing (74) in (27), the PDF of $\gamma_1 > 0$ can be rewritten as

$$f_{\gamma_1}(\gamma_1) = \frac{1}{2\bar{\gamma}_1} \sum_{j=0}^{\infty} \left(a_j(\alpha,\beta) \left(\frac{\gamma_1}{\bar{\gamma}_1}\right)^{\frac{j+\beta}{2}-1} + a_j(\beta,\alpha) \left(\frac{\gamma_1}{\bar{\gamma}_1}\right)^{\frac{j+\alpha}{2}-1} \right), \ (\alpha-\beta) \notin \mathbb{Z} \tag{75}$$

where

$$a_j(\alpha,\beta) \triangleq \frac{\pi(\alpha\beta)^{j+\beta}}{\sin\left[\pi\left(\alpha-\beta\right)\right]\Gamma\left(\alpha\right)\Gamma\left(\beta\right)\Gamma\left(j-\alpha+\beta+1\right)j!} \tag{76}$$

A power series representation for the outage probability of the FSO subsystem can be found by integrating (75) from 0 to γ_{th1}. As a result, we get

$$P_{out,FSO}(P_t) = \sum_{j=0}^{\infty} \left(\frac{a_j\left(\alpha,\beta\right)}{j+\beta} \left(\frac{h_{\ell 1}P_1}{P_{th1}}\right)^{-j-\beta} + \frac{a_j\left(\beta,\alpha\right)}{j+\alpha} \left(\frac{h_{\ell 1}P_1}{P_{th1}}\right)^{-j-\alpha} \right) \tag{77}$$

for $P_1 = P_t \ / \ 2$. Since (77) is an infinite series, the question of convergence arises. For this purpose, we may apply the ratio test to calculate the convergence radius R_1 of the first subseries in (77) as

$$\begin{aligned} R_1 &= \lim_{j\to\infty} \left| \frac{a_j(\alpha,\beta)}{a_{j+1}(\alpha,\beta)} \frac{j+1+\beta}{j+\beta} \left(\frac{h_{\ell 1}P_1}{P_{th1}}\right) \right| \\ &= \lim_{j\to\infty} \frac{\left(j-\alpha+\beta+1\right)\left(j+1\right)\left(j+1+\beta\right)}{\alpha\beta\left(j+\beta\right)} \left(\frac{h_{\ell 1}P_1}{P_{th1}}\right) \to \infty \end{aligned} \tag{78}$$

Similarly, we obtain for the convergence radius R_2 of the second subseries in (77) $R_2 \to \infty$. Therefore, (77) absolutely converges for all $P_t < \infty$.

In practice, some finite value J has to be used for the upper limit of the sum in (77) and we denote the resulting outage probability approximation by $P_{out,FSO}(P_t, J)$.

As shown in Appendix C, the approximation error defined as $\varepsilon_1(J) \triangleq |P_{out,FSO}(P_t) - P_{out,FSO}(P_t, J)|$ is bounded by

$$\varepsilon_1(J) < \frac{\pi \xi_{\max} x_0^{J+1} e^{x_0}}{|\sin[\pi(\alpha-\beta)]|\,\Gamma(\alpha)\,\Gamma(\beta)\,(J+1)!} \tag{79}$$

where

$$\xi_{\max} \triangleq \max_{j>J} \left| \frac{x_0^{\beta}}{(j+\beta)\,\Gamma(j-\beta+\alpha+1)} - \frac{x_0^{\alpha}}{(j+\alpha)\,\Gamma(j-\alpha+\beta+1)} \right| \tag{80}$$

with $x_0 = \alpha\beta P_{th1}/h_{\ell 1} P$. The upper bound in (79) illustrates that the approximation error can be made arbitrarily small by increasing J and/or P_t. Thus, since the coefficients of the series in (79) only involve ordinary functions and $\Gamma(\cdot)$, the truncated version of (79) can be used for fast performance evaluation of the FSO subsystem with Gamma-Gamma fading.

4.3.2 Outage Probability of RF Subsystem

For the RF subsystem with Rician fading, the corresponding outage probability is given by (63) in terms of the first-order Marcum Q-function $Q_1(\cdot,\cdot)$. Here, we present the derivation of a power series expansion for the expression in (63).

We make use of a power series expansion for the first-order Marcum Q-function that is [52, Eqs. 2.3, 2.5]

$$Q_1\left(\sqrt{2x}, \sqrt{2y}\right) = 1 - \sum_{n=0}^{\infty} (-1)^n e^{-a} \frac{L_n(x)}{\Gamma(v+n+1)} y^{n+v} \tag{81}$$

which holds for all $a > 0$ and $b \geq 0$. In (81), L_n is the Laguerre polynomial of degree n, defined explicitly as [20, Eq. 8.970-1, -2]

$$L_n(x) = \sum_{m=0}^{n} \binom{n}{m} \frac{(-x)^m}{m!} \tag{82}$$

Combining (81) with (63), a power series representation for the outage probability of the RF subsystem can be obtained as

$$P_{out,RF}(P_t) = \sum_{n=0}^{\infty} (-1)^n e^{-K} \frac{L_n(K)}{(n+1)!} \left(\frac{1}{(K+1)} \frac{h_{\ell 2} P_2}{P_{th2}} \right)^{-n-1} \tag{83}$$

for $P_2 = P_t$ / 2. The absolute convergence of the infinite series in (83) can be shown by using the following inequalities

$$\begin{aligned}
&\left| \sum_{n=0}^{\infty} (-1)^n e^{-K} \frac{L_n(K)}{(n+1)!} \left(\frac{1}{(K+1)} \frac{h_{\ell 2} P_2}{P_{th2}} \right)^{-n-1} \right| \\
&\leq e^{-K} \sum_{n=0}^{\infty} \frac{1}{(n+1)!} \left(\frac{1}{(K+1)} \frac{h_{\ell 2} P_2}{P_{th2}} \right)^{-n-1} |L_n(K)| \\
&\leq \exp\left(\frac{(K+1)\, P_{th2}}{h_{\ell 2} P_2} - \frac{K}{2} \right)
\end{aligned} \tag{84}$$

which contains the known inequality of $|L_n(x)| \leq e^{x/2}$ for Laguerre polynomials [52]. Thus, (83) absolutely converges for all $P_t < \infty$.

For analytical calculations, some finite number of terms $J+1$ is enough for efficient computation of the sum in (83) and we denote the approximated outage probability by $P_{out,RF}(P_t, J)$. It is proved in Appendix C that the corresponding approximation error defined as $\varepsilon_2(J) \triangleq |P_{out,RF}(P_t) - P_{out,RF}(P_t, J)|$ can be bounded by

$$\varepsilon_2(J) < \frac{y_0^{J+2} e^{y_0 - K/2}}{(J+2)!} \tag{85}$$

where $y_0 \triangleq (K+1) P_{th2} / h_{\ell 2} P_2$. Using the upper bound in (85), the approximation error can be made arbitrarily small by increasing J and/or P_t. Therefore, since the coefficients of the series in (85) only perform ordinary operations and functions, the truncated form of (85) can be utilized for quick performance assessments of the RF subsystem with Ricain fading.

4.3.3 Asymptotic Analysis

Here, we deduce a key result from our generalized power series approximations that plays an important role in deriving the diversity gain of multi-hop hybrid FSO/RF systems. This requires asymptotic analysis of the outage probability results. Specifically, we need to find asymptotical expressions for outage probabilities of the FSO and RF subsystems as the transmit power $P_t \to \infty$. From (77), it is observed that for large values of P_t the higher order terms have negligible contribution in the sum

and, as a result, the first term (i.e., for $j = 0$) is dominant. Thus, (77) asymptotically approaches to

$$P_{out,FSO}\left(P_t\right) \approx \frac{a_0\left(\max\{\alpha,\beta\},\min\{\alpha,\beta\}\right)}{\min\{\alpha,\beta\}}\left(\frac{h_{\ell 1}P_1}{P_{th1}}\right)^{-\min\{\alpha,\beta\}} \tag{86}$$

Similarly, as $P_t \to \infty$, the first term of the sum in (83) (i.e., for $n = 0$) become dominant. Therefore, (83) asymptotically approaches to

$$P_{out,RF}\left(P_t\right) \approx e^{-K}\left(\frac{h_{\ell 2}P_2}{\left(K+1\right)P_{th2}}\right)^{-1} \tag{87}$$

for $P_1 = P_2 = P_t \ / \ 2$.

4.4 Diversity Gain Analysis

In the wireless communication literature for either FSO or RF systems, it is customary to characterize fading channels in terms of their diversity gain [51], [35]. The diversity gain is conventionally defined as the slope of the error or outage performance curve on a log-log scale in the asymptotic regime for SNR $\to \infty$ [49]. Particularly, in our case, the diversity gain G_d can be defined as

$$G_d \triangleq -\lim_{P_t\to\infty}\frac{\log P_{out}\left(P_t\right)}{\log P_t} \tag{88}$$

In this section, we present the diversity gain analysis for multi-hop hybrid FSO/RF systems based on (88). In the following, we begin with the single-hop hybrid FSO/RF system and, subsequently, we go over the multi-hop case.

4.4.1 Single-Hop FSO/RF System

For the multi-hop hybrid FSO/RF system under consideration, the asymptotic outage probability expression $P_{out,Hyb,i}$ of the i^{th} hybrid FSO/RF link, for $i = 1, 2, \ldots, N+1$, is obtained by replacing (86) and (87) in (72) as

$$P_{out,Hyb,i}\left(P_t\right) \approx s\left(\ell_i\right)P_t^{-\min\{\alpha(\ell_i),\beta(\ell_i)\}-1} \tag{89}$$

where

$$s\left(\ell_i\right) \triangleq \frac{a_0\left(\max\left\{\alpha\left(\ell_i\right),\beta\left(\ell_i\right)\right\},\min\left\{\alpha\left(\ell_i\right),\beta\left(\ell_i\right)\right\}\right)}{\min\left\{\alpha\left(\ell_i\right),\beta\left(\ell_i\right)\right\}} \times\left(\frac{2\left(N+1\right)P_{th1}}{h_{\ell 1}\left(\ell_i\right)}\right)^{\min\{\alpha(\ell_i),\beta(\ell_i)\}}\left(\frac{2\left(N+1\right)\left(K+1\right)P_{th2}}{e^K h_{\ell 2}\left(\ell_i\right)}\right) \tag{90}$$

Inserting (89) in (88), the corresponding diversity gain $G_{d,Hyb,i}$ is found as

$$G_{d,Hyb,i} = \min\left\{\alpha\left(\ell_i\right),\beta\left(\ell_i\right)\right\}+1 = G_{d,FSO,i}+G_{d,RF,i} \tag{91}$$

where $G_{d,FSO,i} = \min\left\{\alpha\left(\ell_i\right),\beta\left(\ell_i\right)\right\}$ and $G_{d,RF,i}=1$ are obtained as diversity gains of the i^{th} FSO and RF links, respectively.

4.4.2 Multi-Hop FSO/RF System

The asymptotic outage probability P_{out} of the multi-hop hybrid FSO/RF system can be found by substituting (89) into the upper bound in (73), which gives

$$P_{out}\left(P_t\right) \approx \sum_{i=1}^{N+1} s\left(\ell_i\right) P_t^{-\min\{\alpha(\ell_i),\beta(\ell_i)\}-1} \tag{92}$$

Assuming the consecutive terminals are placed equidistant along the path from the source to the destination, we have $\ell_i = L/(N+1)$ for $i = 1,2,\ldots,N+1$. Consequently, (92) is further simplified as

$$P_{out}\left(P_t\right) \approx \left(N+1\right) P_t^{-\min\{\alpha(L/(N+1)),\beta(L/(N+1))\}-1} \tag{93}$$

Inserting (93) in (88), the diversity gain G_d of the multi-hop hybrid FSO/RF system is derived as

$$G_d = G_{d,FSO}+G_{d,RF} \tag{94}$$

where $G_{d,FSO}$ and $G_{d,RF}$ are diversity gains of the FSO and RF subsystems, which are given by

$$G_{d,FSO} = \min\left\{\alpha\left(L/(N+1)\right),\beta\left(L/(N+1)\right)\right\} \tag{95}$$

$$G_{d,RF} = 1 \tag{96}$$

The expressions in (95) and (96) clarify that diversity gain of the multi-hop system comes from the FSO subsystem since the diversity gain of the RF counterpart is always constant independent of the link distance. Notice that the parameters $\alpha(\cdot)$ and $\beta(\cdot)$ are monotonically decreasing with increasing the link distance. Thus, for a fixed end-to-end service length L the diversity gain increases with increase in the number of deployed relays N.

4.4.3 Special Case of FSO Point-Receiver

Here, we consider a special case for the diversity gain of the FSO subsystem in (95) when the receiver aperture diameter of the FSO subsystems is negligible comparing to the link distance for every hop, i.e., as $(N+1)\,D/L \to 0$. In such a case, it is observed from (13) and (14) that the Gamma-Gamma fading parameters α and β for a sufficiently large number of relays (i.e., $N \gg 1$) can be approximated as

$$\alpha\left(L/(N+1)\right) \approx \frac{(N+1)^{11/6}}{0.49\chi^2\left(L\right)} \tag{97}$$

$$\beta\left(L/(N+1)\right) \approx \frac{(N+1)^{11/6}}{0.51\chi^2\left(L\right)} \tag{98}$$

where $\chi^2\left(L\right) = 0.5C_n^2k^{7/6}L^{11/6}$ is the Rytov variance for spherical wave propagation as defined earlier in chapter 2. Combining (97) and (98) with (95), we deduce

$$G_{d,FSO} \approx \frac{2(N+1)^{11/6}}{\chi^2\left(L\right)} \tag{99}$$

The approximation in (99) shows that when $N \gg 1$ the diversity gain of the FSO subsystem scales proportional with $(N+1)^{11/6}$. At the same time for $N \gg 1$, the scintillation index in (10) reduces to

$$\sigma_I^2 \approx \frac{\chi^2\left(L\right)}{(N+1)^{11/6}} = \chi^2\left(L/(N+1)\right) \tag{100}$$

Interestingly, when we use (100) for [52, Eq. 34], the result is equal to $(N+1)^{11/6}$ which has been found in [52, Eq. 36] as the relative diversity order ARDO $\triangleq$ $\chi^2\left(L\right)/\chi^2\left(L/(N+1)\right)$ for multi-hop FSO systems in Log-normal fading channels.

4.4.4 Numerical Results

In this section, we present our numerical results for asymptotic and diversity gain analyses of multi-hop hybrid FSO/RF systems. We assume point receiver for FSO subsystem, which implies the aperture diameter of $D \approx 0$. All other parameters of the FSO and RF subsystems and weather-dependent variables are set by Tables 1 and 2. Outage performance results are plotted versus the total transmit power P_t.

Figs. 20 and 21 demonstrate the outage probability of a single-hop FSO link in clear weather and haze conditions, respectively. For these figures, we assume a point-to-point link distance of 2 km. Outage probability results are plotted based on (61) for Log-normal fading (LN), (77) for approximated Gamma-Gamma fading ($\Gamma\Gamma$) and (86) for asymptotic Gamma-Gamma fading. Simulation results based on the exact computation of (44) are also provided for comparison purposes. From Figs. 20-21, it is observed that the approximated outage probability with a truncation limit of $J = 20$ perfectly follows the simulation result under both clear weather and haze conditions. It is also observed that there is a significant difference between the plots for Log-normal fading with respect to Gamma-Gamma fading especially in clear weather condition. In fact, the most severe turbulence strength occurs during a clear weather for which the Rytov variance $\sigma_R^2 > 1$ and, therefore, the Log-normal fading model is no more valid. As Figs. Figs. 20-21 clearly illustrate, the asymptotic outage probability results well approach to the actual curves as P_t increases for both shown weather conditions. These observations reveal our robust approximation of the outage probability for Gamma-Gamma fading channels.

Figs. 22 and 23 illustrate the outage probability of a single-hop hybrid FSO/RF system in clear weather and haze conditions, respectively. For these figures, all parameters settings are the same as done for Figs. 20-21. The performances of individual FSO and RF links are shown to compare with the hybrid FSO/RF system under consideration. As a benchmark, simulation results are also included based on the exact

computation of (44) for individual FSO link and (43) for hybrid FSO/RF system. Approximated outage probability results are demonstrated based on the calculation of (77) within a truncation by for FSO link. Asymptotic outage performance results of the hybrid FSO/RF system are evaluated using (89). From Figs. 22-23, first of all it can be observed that the approximated outage probability results for hybrid FSO/RF system are in excellent agreement with the simulation results. It is also observed that the asymptotic outage performance of the hybrid FSO/RF system closely follows the actual curve for both clear weather and haze conditions. The observations from Figs. 22-23 verify our robust approximation and asymptotic analyses for single-hop hybrid FSO/RF system.

To present the diversity gain results, we plot the "diversity ratio" defined as the ratio $-\log P_{out}/\log P_t$ based on (88) with respect to the total transmit power P_t. Figs. 24 and 25 demonstrate the diversity ratio of the multi-hop hybrid FSO/RF system under clear weather condition with $N = 1$ and $N = 2$ number of relays, respectively. For these figures, an end-to-end link distance of $L = 5$ km is considered. The performance of multi-hop FSO and multi-hop RF systems with the same configuration as the multi-hop hybrid FSO/RF system are shown for comparison purposes. From Figs. 24-25, it is overall observed that the diversity ratios significantly increase with increasing the number of the deployed relays along the communication path between the source and the destination. Another observation can be made for the higher diversity ratios of the multi-hop hybrid FSO/RF system with reference to the multi-hop FSO or RF systems in every figure. For the case of $N = 1$ (i.e., dual-hop transmission), the diversity ratios converge to 2.87, 1.83 and 1.13 for multi-hop hybrid FSO/RF, multi-hop FSO and multi-hop RF systems, correspondingly, which match to the derived diversity gains of $G_d = 2.63$, $G_{d,FSO} = 1.63$ and $G_{d,RF} = 1$, cf. (94)-(96). For $N = 2$, we have asymptotic diversity ratios of 4.00, 2.82 and 1.26 in the high P_t regime matching to $G_d = 3.50$, $G_{d,FSO} = 2.50$ and $G_{d,RF} = 1$, respectively.

Fig. 26 demonstrates the diversity ratio of a dual-hop hybrid FSO/RF system (i.e., $N = 1$) under haze condition. Similar to Figs. 24-25, the diversity ratio of the multi-hop hybrid FSO/RF system is improved with respect to the multi-hop FSO or RF systems. In Fig. 26, the diversity ratios of the multi-hop hybrid FSO/RF, multi-hop FSO and multi-hop RF systems converge to 4.41, 3.36 and 1.13, respectively, which are consistent with the diversity gain results of $G_d = 4.20$, $G_{d,FSO} = 3.20$ and $G_{d,RF} = 1$.

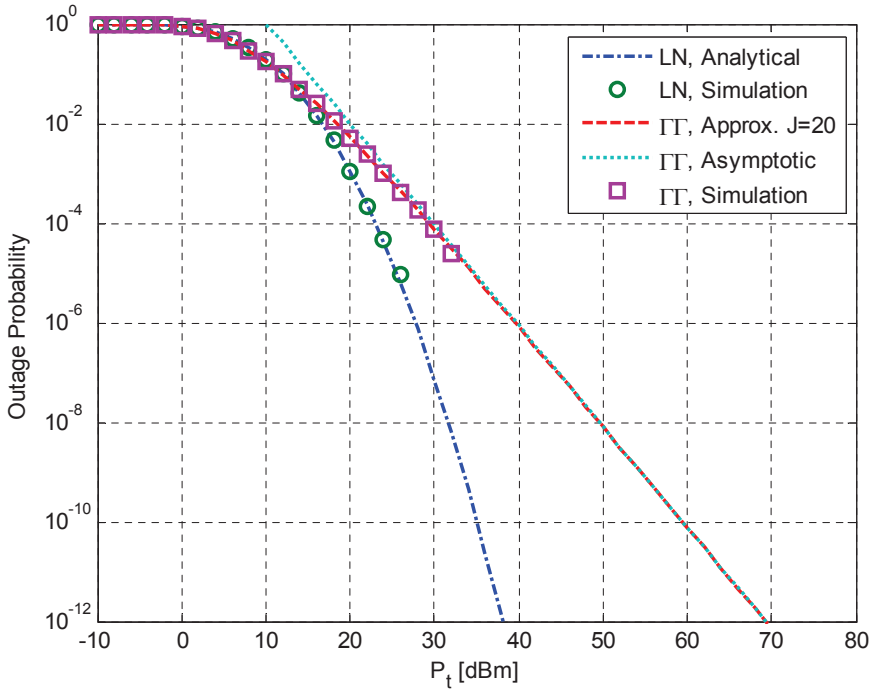

Figure 20: Outage probability of single-hop FSO link under clear weather condition.

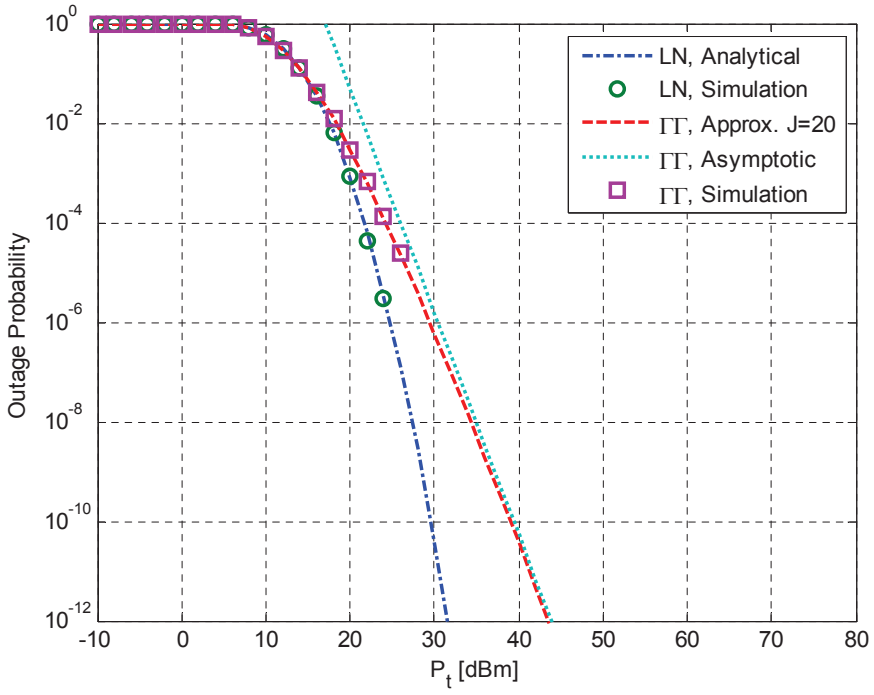

Figure 21: Outage probability of single-hop FSO link under haze condition.

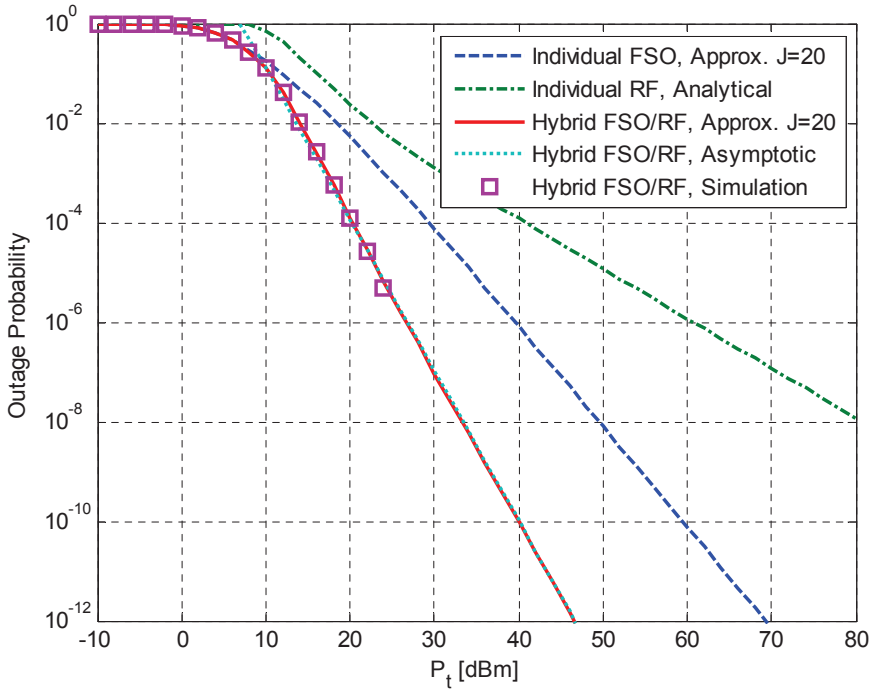

Figure 22: Outage probability of single-hop hybrid FSO/RF system under clear weather condition.

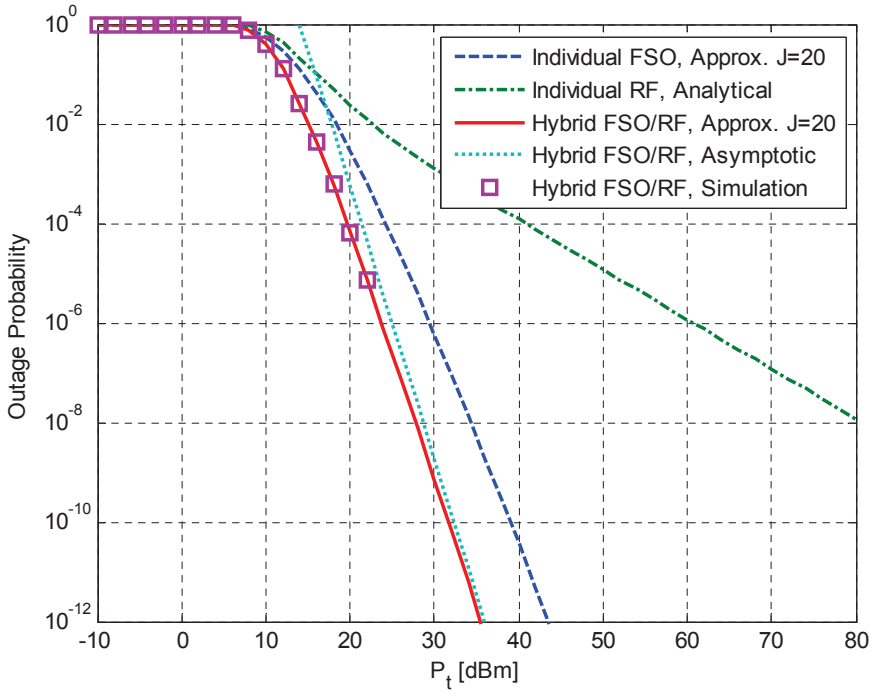

Figure 23: Outage probability of single-hop hybrid FSO/RF system under haze condition.

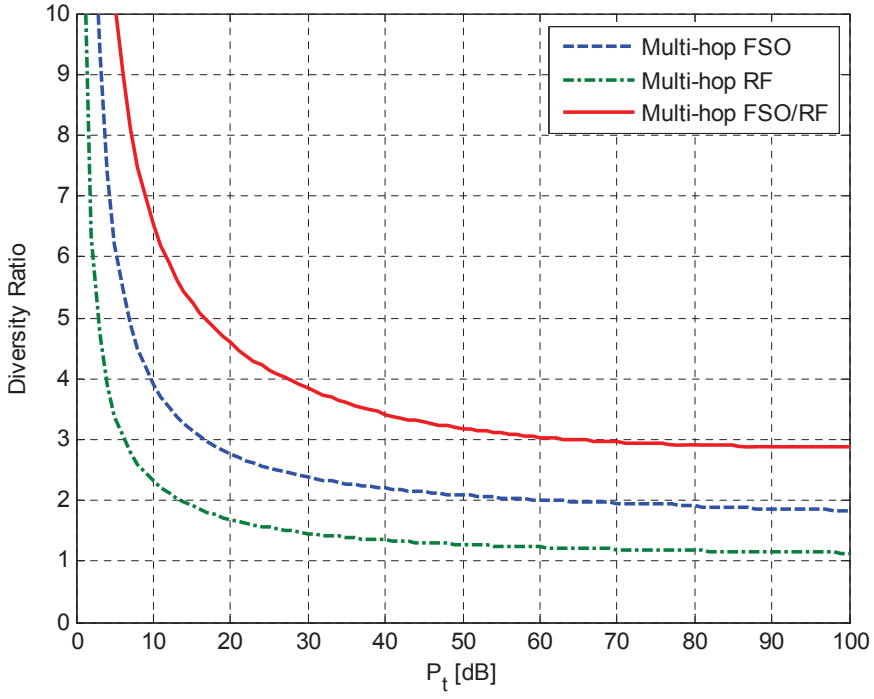

Figure 24: Diversity ratio of multi-hop hybrid FSO/RF system for $N = 1$ under clear weather condition.

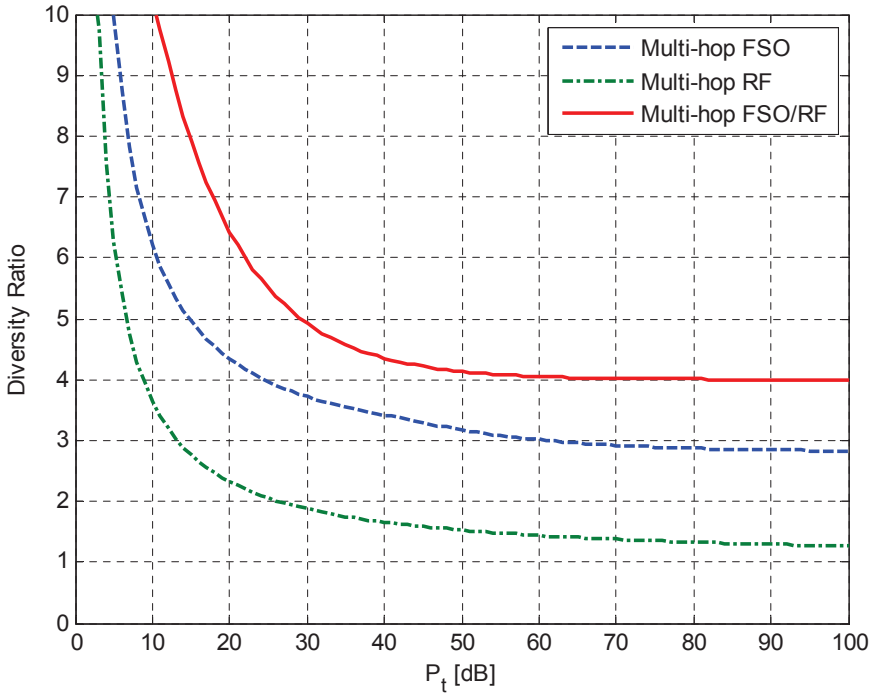

Figure 25: Diversity ratio of multi-hop hybrid FSO/RF system for $N = 2$ under clear weather condition.

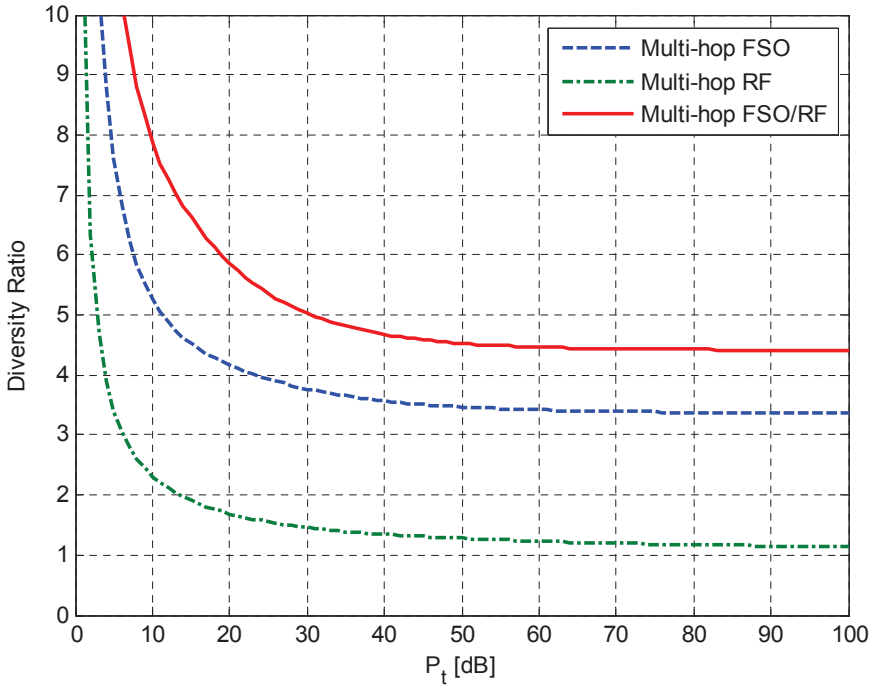

Figure 26: Diversity ratio of multi-hop hybrid FSO/RF system for $N = 1$ under haze condition.

CHAPTER V

CONCLUSIONS

5.1 Main Results of the Thesis

The main results achieved in this thesis are listed as follows:

- An FSMC model was proposed for soft-switching hybrid FSO/RF systems.
- Closed-form outage probability expressions were derived. It was proved that the outage probability of the soft-switching hybrid FSO/RF system is equal to the product of the outage probabilities for individual FSO and RF links. Using the derived expressions, performance improvements of hybrid FSO/RF systems with respect to stand-alone FSO and RF links in different weather conditions were shown.
- Outage capacity of the hybrid FSO/RF system was derived based on the FSMC model. It was shown that the outage capacity of the soft-switching hybrid FSO/RF system is equal to the summation of the outage capacities of the individual FSO and RF channels.
- For multi-hop hybrid FSO/RF communication systems with DF relaying protocol, the optimum (i.e., the most reliable) scenario to forward the signal from the source to the destination, was found. The optimum scenario was found as the one which deploys a hybrid FSO/RF link for every intermediate hop to maximize the end-to-end reliability of the system.
- Robust approximation formula for the outage probability of multi-hop hybrid FSO/RF systems was derived through generalized power series expansions of the outage probabilities for single-hop FSO and RF links.
- Diversity gain of the multi-hop hybrid FSO/RF system was derived. It was

shown that the resulting diversity gain is equal to the summation of diversity gains individually offered by each FSO and RF subsystem. Furthermore, it was found that the diversity gain of the multi-hop hybrid FSO/RF system comes from the FSO subsystem since the diversity gain of the RF counterpart is always constant (i.e., unity) independent of the link distance.

- As a special case, the ADRO of the multi-hop hybrid FSO system in log-normal fading channels was deduced from the presented diversity gain analysis for Gamma-Gamma fading channels.

5.2 Future Directions

In this section, we address a number of research proposals based on the contents of this dissertation.

Outage Capacity of Soft-switching Hybrid FSO/RF Systems with Channel Coding

The fundamental outage capacity bound for hybrid FSO/RF systems were found in chapter 3 of this thesis. From information theory, the derived bound can be achieved using a strong channel coding scheme. Understanding the relationship between the derived capacity bound and the achieved capacity bound using some channel coding scheme in a realistic scenario where we have a "hybrid receiver", can be an interesting topic for future work. This involves a deep theoretical research as well as practical implementations. The comprehensive hybrid FSO/RF channel and link selection models presented in this thesis are useful for this purpose.

Optimal Relay Placement for Multi-Hop Hybrid FSO/RF Systems

In chapter 4 of this thesis, we concluded the optimum scenario for multi-hop transmissions through hybrid FSO/RF links. While we considered the optimum scenario with equidistant hops, a question may arise, is this the best that we can do for maximizing the end-to-end reliability of the system? In a response to this question, a research

topic can be defined as another future work accordingly. Specifically, the potential research involves the investigation of various possible configurations to realize multi-hop hybrid FSO/RF systems. The required mathematical analysis may engage some nonlinear optimization method to find the solution.

APPENDIX A

STANDARD VISIBILITY RANGES FOR DIFFERENT WEATHER CONDITIONS

The visibility ranges for different weather conditions, specified in International Visibility Code weather conditions and precipitation [4], are listed in Table 6.

Table 6: Defined visibility ranges for different weather conditions.

<table>
<tr><th>Weather Condition</th><th colspan="2">Precipitation [mm/h]</th><th>Visibility</th></tr>
<tr><td rowspan="2">Dense Fog</td><td colspan="2"></td><td>0 m</td></tr>
<tr><td colspan="2"></td><td>50 m</td></tr>
<tr><td>Thick Fog</td><td colspan="2"></td><td>200 m</td></tr>
<tr><td>Moderate Fog</td><td rowspan="8">Snow</td><td></td><td>500 m</td></tr>
<tr><td>Light Fog</td><td>Cloudburst 100</td><td>770 m</td></tr>
<tr><td rowspan="2">Thin Fog</td><td></td><td>1 km</td></tr>
<tr><td>Heavy rain 25</td><td>1.9 km</td></tr>
<tr><td rowspan="2">Haze</td><td></td><td>2 km</td></tr>
<tr><td>Moderate rain 12.5</td><td>2.8 km</td></tr>
<tr><td rowspan="2">Light Haze</td><td></td><td>4 km</td></tr>
<tr><td>Light rain 2.5</td><td>5.9 km</td></tr>
<tr><td rowspan="2">Clear</td><td colspan="2"></td><td>10 km</td></tr>
<tr><td colspan="2">Drizzle 0.25</td><td>18.1 km</td></tr>
<tr><td rowspan="3">Very Clear</td><td colspan="2"></td><td>20 km</td></tr>
<tr><td colspan="2"></td><td>23 km</td></tr>
<tr><td colspan="2"></td><td>50 km</td></tr>
</table>

APPENDIX B

OUTAGE PROBABILITY OF FSO SUBSYSTEM IN GAMMA-GAMMA FADING

In this appendix, we present the derivation of the outage probability for FSO subsystem in Gamma-Gamma fading as given in (28). To this end, we need to find the CDF of γ_1 with Gamma-Gamma distribution by integrating its PDF in (26). Let us write the modified Bessel function $K_v(x)$ in terms of the Meijer's G-function as [54, Eq. 14]

$$K_v(x) = \frac{1}{2} G_{1,3}^{2,1}\left[\frac{x^2}{4} \middle| \begin{matrix} - \\ \frac{v}{2}, -\frac{v}{2} \end{matrix} \right] \tag{101}$$

the CDF of γ_1 can be derived by integrating (26) from zero to infinity with the help of [54, Eq. 26] and [20, Eq. 9.31-5] as

$$F_{\gamma_1}(\gamma_{th1}) = \frac{1}{\Gamma(\alpha)\Gamma(\beta)} G_{1,3}^{2,1}\left[\alpha\beta\sqrt{\frac{\gamma_{th1}}{\bar{\gamma}_1}} \middle| \begin{matrix} 1 \\ \alpha, \beta, 0 \end{matrix} \right] \tag{102}$$

Finally, by expanding the average SNR $\bar{\gamma}_1$ in terms of the transmit power P_1 as in (24), the outage probability of the FSO subsystem in Gamma-Gamma fading is found as

$$P_{out,FSO}\left(P_1\right) = \frac{1}{\Gamma(\alpha)\Gamma(\beta)} G_{1,3}^{2,1}\left[\frac{\alpha\beta P_{th1}}{h_{\ell 1} P_1} \middle| \begin{matrix} 1 \\ \alpha, \beta, 0 \end{matrix} \right] \tag{103}$$

Notice that the Meijer G-function [20, Eq. 9.301] is a standard built-in function in most of the well-known mathematical software packages such as Mathematica and Maple.

APPENDIX C

TRUNCATION ERROR ANALYSIS

In this appendix, we develop analytical upper bounds for truncation errors of the approximated outage probability expressions corresponding to FSO and RF subsystems.

The approximation error $\varepsilon_1(J) \triangleq |P_{out,FSO}(P_t) - P_{out,FSO}(P_t, J)|$ can be expressed as

$$\varepsilon_1(J) = \frac{\pi}{|\sin[\pi(\alpha-\beta)]|\,\Gamma(\alpha)\,\Gamma(\beta)} \left| \sum_{j=J+1}^{\infty} \xi_j \frac{x_0^j}{j!} \right| \tag{104}$$

where $\xi_j \triangleq u_j(\alpha,\beta) - u_j(\beta,\alpha)$, $u_j(\alpha,\beta) \triangleq {x_0}^{\beta}/(j+\beta)\Gamma(j-\beta+\alpha+1)$, and $x_0 \triangleq \alpha\beta P_{th1}/h_{\ell 1}P_1$. After some algebraic manipulations from calculus, $\varepsilon_1(J)$ in (104) can be bounded by

$$\begin{aligned} \varepsilon_1(J) &< \frac{\pi\xi_{\max}}{|\sin[\pi(\alpha-\beta)]|\,\Gamma(\alpha)\,\Gamma(\beta)} \left| \sum_{j=J+1}^{\infty} \frac{x_0^j}{j!} \right| \\ &< \frac{\pi\xi_{\max} x_0^{J+1} e^{x_0}}{|\sin[\pi(\alpha-\beta)]|\,\Gamma(\alpha)\,\Gamma(\beta)\,(J+1)!} \end{aligned} \tag{105}$$

where $\xi_{\max}$ is defined as $\xi_{\max} \triangleq \max_{j>J} |\xi_j|$. It can be shown that there is a $j_0 \geq J$ such that ξ_j monotonically decreases for $j > j_0$. Therefore, the quantity $\xi_{\max}$ can be easily computed. Note that for sufficiently large J, $j_0 = J$ holds.

On the other hand, the approximation error $\varepsilon_2(J) \triangleq |P_{out,RF}(P_t) - P_{out,RF}(P_t, J)|$ can be written as

$$\varepsilon_2(J) = e^{-K} \left| \sum_{n=J+1}^{\infty} \zeta_j \frac{y_0^{n+1}}{(n+1)!} \right| \tag{106}$$

where $\zeta_j \triangleq (-1)^n L_n(K)$, and $y_0 \triangleq (K+1)P_{th2}/h_{\ell 2}P_2$. From (106), we observe that

$\varepsilon_2(J)$ can be bounded as

$$\varepsilon_2(J) < e^{-K}\zeta_{\max}\left|\sum_{n=J+1}^{\infty}\frac{y_0^{n+1}}{(n+1)!}\right| < \frac{y_0^{J+2}e^{y_0-K/2}}{(J+2)!} \tag{107}$$

where we have used the definition $\zeta_{\max} \triangleq \max_{j>J}|\zeta_j|$, which can be simply calculated based on the known inequality $|L_n(x)| \leq e^{x/2}$ [52] for Laguerre polynomials as $\zeta_{\max} = e^{K/2}$.

We found that in practice $J \geq 20$ is sufficient for typical values of α, β and K.

Bibliography

[1] L. C. Andrews and R. L. Phillips, *Laser Beam Propagation through Random Media*. SPIE Publications, 2nd ed., 2005.

[2] D. K. Borah, A. C. Boucouvalas, C. C. Davis, S. Hranilovic, and K. Yiannopoulos, "A Review of Communication-oriented Optical Wireless Systems," *EURASIP J. Wireless Commun. Netw.*, vol. 2012, no. 1, pp. 1–28, March 2012.

[3] D. Kedar and S. Arnon, "Urban Optical Wireless Communication Networks: The main Challenges and Possible Solutions," *IEEE Commun. Magazine*, vol. 42, no. 5, pp. S2–S7, May 2004.

[4] I. I. Kim and E. J. Korevaar, "Availability of Free-Space Optics (FSO) and Hybrid FSO/RF Systems," in *Proc. SPIE Opt. Wireless Commun. IV*, vol. 4530, pp. 84–95, Denver CO, 21-22 August 2001.

[5] W. Zhang, S. Hranilovic, and C. Ce, "Soft-Switching Hybrid FSO/RF Links using Short-Length Raptor Codes: Design and Implementation," *IEEE JSAC*, vol. 27, no. 9, pp. 1698–1708, December 2009.

[6] F. Nadeem, M. Gebhart, E. Leitgeb, W. Kogler, M. S. Awan, M. S. Khan, and G. Kandus, "Simulations and Analysis of Bandwidth Efficient Switch-over between FSO and mmW Links," in *Proc. 16th SoftCOM*, pp. 356–361, Croatia, 25-27 September 2008.

[7] Y. Tang, M. Brandt-Pearce, and S. Wilson, "Link Adaptation for Throughput Optimization of Parallel Channels with Application to Hybrid FSO/RF Systems," *IEEE Trans. Commun.*, vol. 60, pp. 2723–2732, September 2012.

[8] B. He and R. Schober, "Bit-Interleaved Coded Modulation for Hybrid RF/FSO Systems," *IEEE Trans. Commun.*, vol. 57, no. 12, pp. 3753–3763, December 2009.

[9] H. Tapse and D. K. Borah, "Hybrid Optical/RF Channels: Characterization and Performance Study using Low Density Parity Check Codes," *IEEE Trans. Commun.*, vol. 57, no. 11, pp. 3288–3297, November 2009.

[10] H. Tapse, D. K. Borah, and J. Perez-Ramirez, "Hybrid Optical/RF Channel Performance Analysis for Turbo Codes," *IEEE Trans. Commun.*, vol. 59, no. 5, pp. 1389–1399, May 2011.

[11] A. Eslami, S. Vangala, and H. Pishro-Nik, "Hybrid Channel Codes for Efficient FSO/RF Communication Systems," *IEEE Trans. Commun.*, vol. 58, no. 10, pp. 2926–2938, October 2010.

[12] A. Akbulut, H. G. Ilk, and F. Ari, "Design,Aavailability and Reliability Analysis on an Experimental Iutdoor FSO/RF Communication System," in *Proc. IEEE Int. Conf. Transparent Opt. Networks*, vol. 1, pp. 403–406, 2005.

[13] A. A. Farid and S. Hranilovic, "Outage Capacity Optimization for Free-Space Optical Links With Pointing Errors," *IEEEE J. Lightw. Technol.*, vol. 25, no. 7, pp. 1702–1710, July 2007.

[14] S. Bloom and W. Hartley, "The Last-Mile Solution: Hybrid FSO Radio," *AirFiber Inc.*, May 2002.

[15] I. I. Kim, B. McArthur, and E. J. Korevaar, "Comparison ofLaser Beam Propagation at 785 nm and 1550 nm in Fog and Haze for Optical Wireless Communications," in *Proc. SPIE*, vol. 4214, pp. 26–37, 2001.

[16] F. Nadeem, V. Kvicera, M. S. Awan, E. Leitgeb, S. Muhammad, and G. Kandus, "Weather Effects on Hybrid FSO/RF Communication Link," *IEEE JSAC*, vol. 27, no. 9, pp. 1687–1697, December 2009.

[17] K. A. Majumdar, "Free-space laser communication performance in the atmospheric channel," *J. Opt. Fiber Commun. Rep.*, vol. 2, no. 4, pp. 345–396, 2005.

[18] M. Uysal, J. Li, and M. Yu, "Error Rate Performance Analysis of Coded Free-Space Optical Links over Gamma-Gamma Atmospheric Turbulence Channels," *IEEE Trans. Wireless Commun.*, vol. 5, no. 6, pp. 1229–1233, June 2006.

[19] M. Al-Habash, R. Phillips, and L. Andrews, "Mathematical model for the irradiance probability density function of a laser beam propagating through turbulent media," *OSA J. Opt. Eng.*, vol. 40, no. 8, pp. 1554–1562, August 2001.

[20] I. S. Gradshtejn and Ryzhik, *Table of Integrals, Series and Products*. Academic Press, 7th ed., New York, USA, 2007.

[21] R. C. Daniels and R. W. Heath, "60 ghz wireless communications: emerging requirements and design recommendations," *IEEE Veh. Technol. Mag.*, vol. 2, no. 3, pp. 41–50, September 2007.

[22] C. Koh, "The Benefits of 60 ghz Unlicensed Wireless Communications," *Whitepaper, Sub10 Systems Ltd*, 2002.

[23] J. Schonthier, "WP3-Study: The 60 GHz Channel and its Modelling," Tech. Rep. IST-2001-32686 Broadway, 2003.

[24] ITU-R, "P. 838-1: Specific Attenuation Model for Rain for Use in Prediction Methods," 1999.

[25] M. K. Simon and M. S. Alouini, *Digital Communication over Fading Channels*. John Wiley & Sons, 2nd ed., 2005.

[26] X. Zhu and J. M. Kahn, "Free-Space Optical Communication through Atmospheric Turbulence Channels," *IEEE Trans. Commun.*, vol. 50, no. 8, pp. 1293–1300, August 2002.

[27] H. Moradi, M. Falahpour, H. H. Refai, P. G. LoPresti, and M. Atiquzzaman, "On the Capacity of Hybrid FSO/RF Links," in *IEEE Global Telecommun. Conf. (GLOBECOM)*, pp. 1–5, 6-10 December 2010.

[28] V. Vishnevskii, O. Semenova, and S. Y. Sharov, "Modeling and Analysis of a Hybrid Communication Channel based on Free-space Optical and Radio-frequency Technologies," *J. Autom. Remote Control*, vol. 74, no. 3, pp. 521–528, March 2013.

[29] N. Letzepis, K. D. Nguyen, A. Guillen i Fabregas, and W. G. Cowley, "Outage analysis of the hybrid free-space optical and radio-frequency channel," *IEEE J. Sel. Areas Commun.*, vol. 27, no. 9, pp. 1709–1719, December 2009.

[30] N. Letzepis, K. D. Nguyen, A. Guillen Fabregas, and W. G. Cowley, "Hybrid Free-Space Optical and Radio-Frequency Communications: Outage Analysis," in *Proc. IEEE Int. Symp. Info. Theory (ISIT)*, pp. 2048–2052, 13-18 June 2010.

[31] H. Wu, B. Hamzeh, and M. Kavehrad, "Achieving Carrier Class Availability of FSO Link via a Complementary RF Link," in *Proc. 38th Asilomar Conf. Signals Syst. Comput.*, vol. 2, pp. 1483–1487, 7-10 November 2004.

[32] H. Moradi, M. Falahpour, H. Refai, P. LoPresti, and M. Atiquzzaman, "Reconfiguration Modeling of Reconfigurable Hybrid FSO/RF Links," in *IEEE Int. Conf. Commun. (ICC)*, pp. 1–5, 23-27 May 2010.

[33] S. Hranilovic, *Wireless Optical Communication Systems*. Springer, 2005.

[34] A. Papoulis and S. U. Pillai, *Probability, Random Variables, and Stochastic Processes*. Tata McGraw-Hill Education, 4th ed., 2002.

[35] A. Goldsmith, *Wireless Communications*. Cambridge University Press, NY, USA, 2005.

[36] S. Vangala and H. Pishro-Nik, "Optimal Hybrid RF-Wireless Optical Communication for Maximum Efficiency and Reliability," in *Proc. 41st Conf. Info. Sciences Syst. (CISS)*, pp. 684–689, 14-16 March 2007.

[37] M. Safari and M. Uysal, "Relay-Assisted Free-Space Optical Communication," *IEEE Trans. Wireless Commun.*, vol. 7, no. 12, pp. 5441–5449, December 2008.

[38] M. Safari, M. M. Rad, and M. Uysal, "Multi-Hop Relaying over the Atmospheric Poisson Channel: Outage Analysis and Optimization," *IEEE Trans. Commun.*, vol. 60, no. 3, pp. 817–829, March 2012.

[39] T. A. Tsiftsis, H. G. Sandalidis, G. K. Karagiannidis, and N. C. Sagias, "Multihop Free-Space Optical Communications Over Strong Turbulence Channels," in *Proc. IEEE Int. Conf. Commun. (ICC)*, vol. 6, pp. 2755–2759, June 2006.

[40] N. D. Chatzidiamantis, D. S. Michalopoulos, E. E. Kriezis, G. K. Karagiannidis, and R. Schober, "Relay Selection Protocols for Relay-Assisted Free-Space Optical Systems," *IEEE/OSA J. Opt. Commun. Netw.*, vol. 5, no. 1, pp. 92–103, January 2013.

[41] H. Izadpanah, T. Elbatt, V. Kukshya, F. Dolezal, and B. K. Ryu, "High-Availability Free Space Optical and RF Hybrid Wireless Networks," *IEEE Wireless Commun. Mag.*, vol. 10, no. 2, pp. 45–53, April 2003.

[42] D. Wang and A. A. Abouzeid, "Throughput Capacity of Hybrid Radio-Frequency and Free-Space-Optical (RF/FSO) Multi-Hop Networks," in *Proc. IEEE Info. Theory and Applications Workshop*, pp. 3–10, 29 January- 2 February 2007.

[43] D. Wang and A. A. Abouzeid, "Throughput and delay analysis for hybrid radio-frequency and free-space-optical (RF/FSO) networks," *J. Wireless Netw.*, vol. 17, no. 4, pp. 877–892, January 2011.

[44] Y. Tang and M. Brandt-Pearce, "Link Allocation, Routing, and Scheduling for Hybrid FSO/RF Wireless Mesh Networks," *IEEE/OSA J. Opt. Commun. Netw.*, vol. 6, no. 1, pp. 86–95, January 2014.

[45] A. Kashyap, A. Rawat, and M. Shayman, "WSN18-4: Integrated Backup Topology Control and Routing of Obscured Traffic in Hybrid RF/FSO Networks," in *Proc. IEEE Global Telecommun. Conf. (GLOBECOM)*, pp. 1–6, 27 November-1 December 2006.

[46] V. Rajakumar, M. N. Smadi, S. C. Ghosh, T. D. Todd, and S. Hranilovic, "Interference management in wlan mesh networks using free-space optical links," *Journal of Lightwave Technology*, vol. 26, no. 13, pp. 1735–1743, 2008.

[47] F. Ahdi and S. Subramaniam, "Optimal Placement of FSO Links in Hybrid Wireless Optical Networks," in *Proc. IEEE Global Telecommun. Conf. (GLOBECOM)*, pp. 1–6, 5-9 December 2011.

[48] H. Moradi, M. Falahpour, H. Reafi, P. G. LoPresti, and M. Atiquzzaman, "Availability Modeling of FSO/RF Mesh Networks through Turbulence-Induced Fading Channels," in *IEEE Conf. Comput. Commun. Workshops (INFOCOM)*, pp. 1–5, 15-19 March 2010.

[49] J. N. Laneman, D. N. Tse, and G. W. Wornell, "Cooperative Diversity in Wireless Networks: Efficient Protocols and Outage Behavior," *IEEE Trans. Info. Theory*, vol. 50, no. 12, pp. 3062–3080, December 2004.

[50] J. N. Laneman and G. W. Wornell, "Energy-Efficient Antenna Sharing and Relaying for Wireless Networks," in *Proc. IEEE Wireless Commun. Netw. Conf. (WCNC)*, vol. 1, pp. 7–12, IEEE, 23-28 September 2000.

[51] E. Bayaki, R. Schober, and R. K. Mallik, "Performance Analysis of MIMO Free-Space Optical Systems in Gamma-Gamma Fading," *IEEE Trans. Commun.*, vol. 57, no. 11, pp. 3415–3424, November 2009.

[52] "The Generalized Marcum Q-Function: An Orthogonal Polynomial Approach,"

[53] M. A. Kashani, M. Safari, and M. Uysal, "Optimal Relay Placement and Diversity Analysis of Relay-Assisted Free-Space Optical Communication Systems," *IEEE/OSA J. Opt. Commun. Netw.*, vol. 5, no. 1, pp. 37–47, January 2013.

[54] V. S. Adamchik and O. I. Marichev, "The Algorithm for Calculating Integrals of Hypergeometric Type Functions and its Realization in REDUCE System," in *Proc. Int. Conf. Symbolic and Algebraic Comput.*, pp. 212–224, Tokyo, Japan, 1990.